Power enhancement of pontoon-type wave energy convertor via hydroelastic response and variable power take-off system

Zhi Yung Tay , Yanji Wei

PII: S2468-0133(19)30106-8
DOI: https://doi.org/10.1016/j.joes.2019.07.002
Reference: JOES 139

To appear in: *Journal of Ocean Engineering and Science*

Received date: 10 April 2019
Revised date: 19 July 2019
Accepted date: 20 July 2019

Please cite this article as: Zhi Yung Tay , Yanji Wei , Power enhancement of pontoon-type wave energy convertor via hydroelastic response and variable power take-off system, *Journal of Ocean Engineering and Science* (2019), doi: https://doi.org/10.1016/j.joes.2019.07.002

Highlights

- The power generation from a pontoon-type wave energy convertor (WEC) is considered and subjected to regular wave condition
- The pontoon-type WEC comprises of several interconnected floating modules which are connected by line hinges
- The hydroelastic response of the pontoon-type WEC is taken into consideration and solved using the coupled boundary element-finite element method
- It is shown that the power generation from the pontoon-type wave energy convertor could be further enhanced via its structural deformation and by utilizing a variable power take-off (PTO) system
- The optimal PTO value is obtained by using the genetic algorithm optimization scheme.

Power enhancement of pontoon-type wave energy convertor via hydroelastic response and variable power take-off system

[1]Zhi Yung Tay[a] and Yanji Wei[b]

[a] Engineering Cluster, Singapore Institute of Technology, 10 Dover Drive, Singapore 138683

[b] Faculty of Science and Engineering, University of Groningen, Nijenborgh 4, Groningen, 9747AG the Netherlands

Abstract

Wave energy has gained its popularity in recent decades due to the vast amount of untapped wave energy resources. There are numerous types of wave energy convertor (WEC) being proposed and to be economically viable, various means to enhance the power generation from WECs have been studied and investigated. In this paper, a novel pontoon-type WEC, which is formed by multiple plate-like modules connected by hinges, are considered. The power enhancement of this pontoon-type WEC is achieved by allowing certain level of structural deformation and by utilizing a series of optimal variable power take-off (PTO) system. The wave energy is converted into useful electricity by attaching the PTO systems on the hinge connectors such that the mechanical movements of the hinges could produce electricity. In this paper, various structural rigidity of the interconnected modules are considered by changing the material Young's modulus in order to investigate its impact on the power enhancement. In addition, the genetic algorithm optimization scheme is utilized to seek for the optimal PTO damping in the variable PTO system. It is observed that under certain condition, the flexible pontoon-type WEC with lesser connection joints is more effective in generating energy as compared to its rigid counterpart with higher connection joints. It is also found that the variable PTO system is able to generate greater energy as compared to the PTO system with constant/uniform PTO damping.

Keywords

Power generation enhancement; pontoon-type wave energy convertor; very large floating structure (VLFS); hydroelastic response; variable power take-off system; genetic algorithm optimization

[1] Corresponding Author, E-mail:zhiyung.tay@singaporetech.edu.sg, Tel: +65 6592 1944

1. Introduction

In order to mitigate the adverse effect of climate change, the International Panel on Climate Change (IPCC) has urged various sectors to reduce their dependency on fossil fuels. As a result, researchers and engineers have looked into other clean energy options such as wind, wave, solar or ocean thermal energy conversion as alternatives to our energy source. The global gross theoretical resource for wave energy has the highest energy density among the renewable energy sources [1] and it is estimated to be 3.7 TW, which is in the same order of magnitude as the global electricity consumption [2]. Thus, this made it an attractive source of alternative energy as a replacement to the fossil fuels and resulted in the various ideation of wave energy convertors (WECs) that convert wave energy to electricity by using power take-off (PTO) systems.

The traditional types of WECs such as the point absorber, attenuator and terminator WECs generate energy via rigid body motion as waves hit on the structures. Recently, the attenuator WEC that is formed by interconnecting several floating modules with a series of PTO system equipped in/between the modules has gained popularity due to its high rated power and capture width ratio. The most well-known being the Pelamis WEC [3] which has a rated power of 750 kW and a capture width ratio of 7%. Other attenuator WECs such as the Ocean Grazer WEC (www.oceangrazer.com) are proposed by researchers from the University of Gronigen to maximize the energy generation from wave via an interconnected array of floating modules connected by hinges.

Researchers have been looking into numerous ways to enhance the performance of the WEC. One of the most common methods is to arrange the WECs in arrays [4-7] in order to maximize the power generation from the wave farm. To further enhance the performance of the wave farm, optimization technique has been performed to seek for the optimal array configuration for the wave farm [8, 9]. In addition, instead of using PTO systems with constant damping value, PTO with variable damping value has been proposed and it appears to improve the performance of the WEC array. This was demonstrated by Wei *et al*. [10] where the authors investigated the Ocean Grazer WEC with ten-hinged connected floating modules where each module is connected by a PTO system with variable PTO damping. Their results showed that the performance of the WEC could be improved significantly through an appropriated PTO array configuration. Also, optimization on the individual PTO system could be performed in order to improve the overall power output, as suggested by de Backer *et al*. [11].

Another novel methodology to enhance the power output of the WEC is to use flexible material for the WEC that generates energy via its flexible motion under wave action termed as the hydroelastic response. Haren and Mei [12] were among the first to propose an analytical model for a train of slender pontoons in a channel with rotational

PTOs attached to the connecting hinges. Another example of a flexible-type attenuator WEC is the Wave Carpet [13] proposed by researchers from the University of Berkeley as means to prevent erosion and protect the harbors by extracting energy from the waves to generate electricity. Other flexible type WECs are such as the Anaconda WEC [14], SBM S3 WEC [15] and Bombora WEC [16] which utilize the structural deformation in generating energy. Zhang *et al*. [17] has also demonstrated the effect of structural flexibility on the power generation of two interconnected floaters.

It is to be noted that most of the aforementioned WEC are long flexible WEC modelled as beam [14, 16-18] whereas the Wave Carpet WEC is a submerged plate-type WEC. So far, limited works on flexible plate-type WEC had been investigated. For example, the Cyprus University of Technology has recently proposed the Water Level Carpet (WLC) WEC [19] which consists of four rectangular shaped floating modules connected flexibly in two directions by connectors with PTO mechanisms where they found that the power production of the WLC obtains large meaningful values for wave frequencies close to the resonance of the generalized degrees of freedom. A novel type of WEC concept has been incorporated in the very large floating structure (VLFS) for the use on ocean space utilization. Zhang *et al*. [20] addressed a flexible runway supported by an array of circular buoy with PTO and claimed that an optimal balance between maximizing wave energy extraction and minimizing the movement of the runway can be achieved with proper stiffness and damping coefficients of PTO. Another recent work by Tay [21] and Nguyen *et al*. [22] investigated a pontoon-type VLFS with an articulated plate that functions both as an antimotion device and a WEC. The author found that it is possible to generate an optimal amount of energy from the wave while keeping a high workability of the articulated plate in minimizing the hydroelastic response.

In view of the effectiveness in power generation enhancement via structural deformation for plate-type WEC, this paper aims to further study and understand the effect of allowing structural deformation in a pontoon-type WEC on the wave energy generation. The considered plate-type WEC is made up of multiple pontoon-type WECs floating on the surface of the water and comprises a grid of floating modules interconnected by line hinges where energy is generated via PTO systems. While a similar flexible raft-type WEC has been considered in [19], which is made up of a two-by-two floating modules, our study shall consider the effectiveness of different module configurations in power generation. Four different configurations of the pontoon-type WECs are considered and described in detail in the following section, with each made up of different numbers of interconnected modules. The effect of structural rigidity of the WEC is simulated using various Young's modulus and structural length. In addition,

a PTO system with variable PTO damping values is considered in order to quantify its effectiveness in enhancing the power generation as compared to its counterpart of a constant/uniform PTO damping value. The genetic algorithm (GA) optimization scheme is used to seek for the optimal variable PTO damping that could maximize the power generation of the WEC. The GA optimisation technique [23], which is a search heuristic that mimics the process of natural selection and involves techniques inspired by natural evolution, such as selection, mutation and crossover, is used as it enhances the computational time in meeting the objective function. The GA will converge over successive generations towards the global optimum via the aforementioned process and has been proven to be a robust tool for optimisation in engineering problem [24]. To the knowledge of the authors, the flexible pontoon-type WEC equipped with variable PTO systems for consideration of power enhancement has not been investigated elsewhere and the results presented shall provide insight on the effectiveness of power enhancement via these two methods.

2. Problem Definition

The paper considers a pontoon-type WEC which consists of a grid of N interconnected floating modules, where each module is connected to each other by using $(N-1)$ line hinge connectors (see Fig 1), i.e. Fig. 1(a) for Type-A with $N = 12$ (11 hinges), Fig. 1(b) for Type-B with $N = 6$ (5 hinges), Fig. 1(c) for Type-C with $N = 4$ (3 hinges) and Fig. 1(d) for Type-D with $N = 1$ (0 hinges). Each pontoon-type module has a length l, breadth B, depth h and is assumed to be made of an isotropic elastic material with a Young's modulus E and mass density ρ_p. The module floats in a draft T_w and on a constant water depth of H. When connected together, the pontoon type WEC has a total length dimension $L = N \times l$, breadth B and depth h. A total of R numbers of PTO system is attached to the WEC to generate energy via the rotational motions of the WEC. The PTO system is spaced at an equal interval of $\frac{L}{12}$ in the horizontal direction ($x-$axis) and $\frac{B}{8}$ in the transverse direction ($y-$axis) as shown in Fig 1, therefore totaling a number of $M = 99$ PTO systems as shown in Figs. 1(a) to (d).

The properties of the pontoon-type WECs and wave condition are shown in Table 1. Three groups of pontoon-type WECs, each with different L are considered, i.e. Group I with $L = 100$ m, Group II with $L = 200$ m and Group III with $L = 300$ m. For each group of the WEC, four types of WEC, i.e. Type-A, -B, -C and -D, each with N different numbers of module, are further considered and depicted in Figs. 1(a) to (d), respectively. It is to be noted that Type-A WEC has the highest number of line hinge connectors, whereas Type- B and -C have a reduced number of line hinge connectors. The Type-D

pontoon-type WEC is a single module WEC and behaves like a continuous mat-like very large floating structures (VLFS). These different types of WECs are subjected to different elastic deformation behavior due to their different module length l and Young's modulus E, thus allowing the investigation of the effect of elastic deformation (i.e. structural rigidity) on the power generation of the WEC. In order to investigate the effect of structural rigidity on the wave energy generation, the WECs in Table 1 are modeled with six different E values, i.e. $E = 0.2$ GPa, 2 GPa, 20 GPa, 200 GPa, 2000 GPa and 20000 GPa. Also, it is to be noted that the total number of PTO systems are kept the same ($R = 99$) for all the WECs considered in Table 1 in order to ensure a fair comparison of the performance of the WECs. Studies will be carried out to investigate the effect of variable PTO damping system in enhancing the power generation of the WEC as compared to its counterpart of a constant PTO damping system. A genetic algorithm optimization technique will be applied to seek for the optimal PTO damping following the scheme presented in [8]. Two cases are considered in the GA optimization to seek for the optimal variable B_{PTO}, i.e. Case 1 where the GA optimization scheme is applied to all the B_{PTO} in the pontoon-type WEC and Case 2 where the GA optimization scheme is applied to the B_{PTO} attached to the line hinge connector only. It is noted here that for the variable PTO system, the B_{PTO} are assumed to vary along the $x-$axis direction but are kept constant for each line connector (along the y-axis direction) in order to reduce the computation time. The scheme will be explained in detail in Section 3.6.

The pontoon-type WEC is subjected to a series of regular waves with a constant wave amplitude $2A$. The wave frequencies ω range from 0.1 rad/s to 1.6 rad/s with an interval of 0.025 rad/s where the regular waves approach the WEC at the head sea direction. The WEC is assumed to operate in a deepwater condition where the effect of seabed on the structural motion is negligible. The particulars and properties of WEC models are given in Table 1. In order to facilitate the discussion, the pontoon-type WEC will be referred to by their Group and Type as summarized in Table 1. For example, a Group I Type-A WEC refers to the 100-meter long pontoon-type WEC interconnected with $N = 12$ floating modules.

3. Mathematical Formulation

The response of the pontoon-type WEC is computed by using the hybrid boundary element–finite element method (BE-FE) developed in MATLAB® where the WEC is modeled as an isotropic plate whereas the fluid is assumed to be inviscid and incompressible and its flow assumed to be irrotational. The global $x-, y-, z-$ axes have the positive direction according to the right hand rule and the origin is located on the center of the WEC, with the $x-y$ plane located at the free surface, i.e. $z = 0$. Figure 2

shows the computational domain of the WEC, where the WEC is assumed to float on the free surface with a constant water depth H. In the BE-FE method, the water domain is represented by Ω, the wetted surface of the WEC by the boundary S_H, the seabed by S_B, the free surface by S_F and the surface at the distance far away from the WEC as $S_{\pm\infty}$. The governing equations for the water and plate as well as the formulation for generated power from the WEC and GA optimization scheme will be presented in the subsequent sections.

3.1 Water Domain

Based on the potential flow theory, the fluid motion may be represented by a velocity potential $\Phi(x, y, z, t)$. We consider the water to oscillate in a steady-state harmonic motion with the circular frequency ω. The velocity potential $\Phi(x, y, z, t)$ could be expressed into the following form:

$$\Phi(x, y, z, t) = Re\{\phi(x, y, z)e^{-i\omega t}\}, \tag{1}$$

The velocity potential $\phi(x, y, z)$ can be expressed as the sum of the diffracted potential ϕ_D and radiated potential by using the linear potential theory, i.e.

$$\phi(x, y, z) = \phi_D + \sum_{l=1}^{P} \zeta_l \phi_l(x, y, z) \tag{2}$$

where the second term in the right hand side of Eq. (2) is the radiated potential expressed as a series of product of P numbers of modal amplitudes ζ_l and the unit-amplitude radiated potential ϕ_l.

The single frequency velocity potential $\phi(x, y, z)$ must satisfy the Laplace equation [25],

$$\nabla^2 \phi = 0 \quad \text{in } \Omega, \tag{3}$$

and the boundary conditions on the surfaces as shown in Fig. 1, which are given as follows [25]:

$$\frac{\partial \phi_l}{\partial z} = \begin{cases} -i\omega w & \text{for } l = 1,2, \dots, P \\ 0 & \text{for } l = D \end{cases} \quad \text{on } S_{HB} \tag{4}$$

$$\frac{\partial \phi_l}{\partial n} = 0 \qquad \text{on } S_{HS} \tag{5}$$

$$\frac{\partial \phi_l}{\partial z} = \frac{\omega^2 \phi}{g} \qquad \text{on } S_F \tag{6}$$

$$\frac{\partial \phi_l}{\partial z} = 0 \qquad \text{on } S_B \tag{7}$$

where n is the unit normal vector to the surface S. The deflection of the pontoon-type WEC w in (4) is described in Section 3.2. It is noted that the hull wetted surface S_H presented in Fig. 2 is divided into the bottom hull wetted surface S_{HB} and the side hull wetted surface S_{HS}, i.e. $S_{HB} \cup S_{HS} \in S_H$. The wave velocity potential must also satisfy the Sommerfield radiation condition at the artificial fluid boundary at infinity S_∞ as $(x, y) \to \infty$ [25]

$$\lim_{|(x,y)\to\infty|} \sqrt{|(x,y)|}\left(\frac{\partial}{\partial |(x,y)|} - ik\right)(\phi_l - \phi_{in}) = 0 \qquad \text{on } S_\infty \tag{8}$$

where k and ϕ_{in} are the standard wave number and incident velocity potential as found in [26]

The Laplace equation (3) together with the boundary conditions (4) to (8) on the surface S are transformed into a boundary integral equation (BIE) by using the Green's Second Theorem via a free surface Green's function. Since the Green's function satisfies the surface boundary condition at the free water surface S_F, the seabed S_B and at the infinity S_∞, only the wetted surface of the bodies S_H need to be discretised into panels so that the boundary element method could be used to solve for the diffracted and radiated potential. For details on the Green's function used in solving the BIE , refer to [26].

3.2 Structure Domain

The pontoon-type WEC on the other hand is modelled as a solid plate by using the Mindlin thick plate theory [27, 28]. The solid plate is simplified to be perfectly flat with free edges and the plate material is commonly assumed to be isotropic and obeys Hooke's Law. The WEC is restraint from moving in the horizontal $x-y$ plane directions by station keeping system and only allowed to move vertically. Hence, the hydroelastic response of the pontoon-type WEC could be described by the deflection $w(x, y)$, the

rotation about the y-axis $\psi_x(x,y)$ and the rotation about the x-axis $\psi_y(x,y)$ as shown in Fig. 3. The governing equations for the Mindlin plate theory are given as follows:

$$\kappa^2 Gh\left[\left(\frac{\partial^2 w}{\partial x^2}+\frac{\partial^2 w}{\partial y^2}\right)+\left(\frac{\partial \psi_x}{\partial x}+\frac{\partial \psi_y}{\partial y}\right)\right]+\rho_p h\omega^2 w = p(x,y) \tag{9}$$

$$D\left[\frac{1-\nu}{2}\left(\frac{\partial^2 \psi_x}{\partial x^2}+\frac{\partial^2 \psi_y}{\partial y^2}\right)+\frac{1+\nu}{2}\left(\frac{\partial^2 \psi_x}{\partial x^2}+\frac{\partial^2 \psi_y}{\partial x \partial y}\right)\right]-\kappa^2 Gh\left(\frac{\partial w}{\partial x}+\psi_x\right)+\rho_p\frac{h^3}{12}\omega^2\psi_x = 0 \tag{10}$$

$$D\left[\frac{1-\nu}{2}\left(\frac{\partial^2 \psi_y}{\partial y^2}+\frac{\partial^2 \psi_x}{\partial x^2}\right)+\frac{1+\nu}{2}\left(\frac{\partial^2 \psi_y}{\partial y^2}+\frac{\partial^2 \psi_x}{\partial x \partial y}\right)\right]-\kappa^2 Gh\left(\frac{\partial w}{\partial y}+\psi_y\right)+\rho_p\frac{h^3}{12}\omega^2\psi_y = 0 \tag{11}$$

where $G = E/[2(1+\nu)]$ is the shear modulus, κ^2 the shear correction factor taken as 5/6, ρ_p the mass density of the plate, h the thickness (i.e. depth) of the plate, $D = Eh^2/[12(1-\nu^2)]$ the flexural rigidity, E the Young's modulus and ν the Poisson ratio. The pressure $p(x,y)$ in Eq. (9) comprises the hydrostatic and hydrodynamic pressure. The boundary conditions at the free edges of the floating plate are

$$M_{nn} = D\left[\frac{\partial \psi_n}{\partial n}+\nu\frac{\partial \psi_s}{\partial s}\right] = 0 \tag{12}$$

$$M_{ns} = D\left(\frac{1-\nu}{2}\right)\left[\frac{\partial \psi_n}{\partial s}+\frac{\partial \psi_s}{\partial n}\right] = 0 \tag{13}$$

$$Q_n = \kappa^2 Gh\left[\frac{\partial w}{\partial n}+\psi_n\right] = 0 \tag{14}$$

where M_{nn}, M_{ns} and Q_n are the bending moment, twisting moment and shear force, respectively. s and n denote the tangential and normal directions to the section of the plate, respectively.

3.3 Continuity Equations for Hinge Connector with PTO system

The continuity equations for the interconnected plate at the hinge connector with PTO damping B_{PTO} located at $(x_c)_{r=1,2,\ldots,R}$ are

$$w|_{x=(x_c^-)_r} = w|_{x=(x_c^+)_r} = 0 \tag{15}$$

$$\psi_y\big|_{x=(x_c^-)_r} = \psi_y\big|_{x=(x_c^+)_r} = 0 \tag{16}$$

$$M_x|_{x=(x_c^-)_r} = M_x|_{x=(x_c^+)_r} = 0 \tag{17}$$

$$M_{xy}\big|_{x=(x_c^-)_r} = M_{xy}\big|_{x=(x_c^+)_r} = 0 \tag{18}$$

$$Q_x|_{x=(x_c^-)_r} = Q_x|_{x=(x_c^+)_r} = 0 \tag{19}$$

These continuity requirements can be implemented into plate elements along the line connection using the standard finite element method. Note that $(x_c^-)_r$ and $(x_c^+)_r$ denote the location at the left and right hand side of the rth PTO system, respectively. Power take-off system is attached at the connector to convert the kinetic energy of the interconnected plate due to wave action to electricity. This is modelled as damper with B_{PTO} along the line hinge connector, i.e. y-axis at $x = (x_c)_r$.

3.4 Equation of Motion for Water-Plate Model

The coupled water-plate problem is solved by using the coupled BE-FE scheme, where the Laplace equation together with the water boundary conditions are solved using the boundary element method whereas the plate equation and its boundary conditions using the finite element method. Due to space constraint, details of the solution scheme are not presented here, but interested readers can refer to the details in [26]. For N numbers of interconnected modules in the pontoon-type WEC, the equation of motion of module p due to module q is written as

$$\{\omega^2(M + M_a) - i\omega[(B_a)_{pp} + B_{PTO}] + (K_f + K_s + K_{rf})\}(\overline{w})_p - \sum_{\substack{q=1 \\ q\neq p}}^{N} [\omega^2(M_a)_{qp} + i\omega(B_a)_{qp}] = (F_e)_p \tag{20}$$

where $\overline{w} = (w, \psi_x, \psi_y)$, M is the mass, K_f the flexural stiffness, K_s the shear stiffness and K_{rf} the restoring force. The added mass M_a, radiated damping B_a and exciting force F_e can be found in [26] and will not be presented here due to its lengthy derivation. Equation (20) can be further transformed into the matrix form to be solved using the

finite element method. The typical B_{PTO} matrix of an interconnected node in the hinge connector is presented as follow

$$B_{PTO} = \begin{array}{c} \\ w \\ \psi_x^- \\ \psi_x^+ \\ \psi_y^- \\ \psi_y^+ \end{array} \begin{array}{c} \begin{array}{ccccc} w & \psi_x^- & \psi_x^+ & \psi_y^- & \psi_y^+ \end{array} \\ \begin{bmatrix} 0 & 0 & 0 & 0 & 0 \\ 0 & 0 & 0 & 0 & 0 \\ 0 & 0 & 0 & 0 & 0 \\ 0 & 0 & 0 & +B_{PTO} & -B_{PTO} \\ 0 & 0 & 0 & -B_{PTO} & +B_{PTO} \end{bmatrix} \end{array} \tag{21}$$

It is noted here that for each node along the line connector, there will be five degrees of freedom, namely $w, \psi_x^-, \psi_x^+, \psi_y^-$ and ψ_y^+. The positive (+) and negative (–) signs denote the right hand side and left hand side of the node in the line connector.

3.5 Generated Power from Anti-Motion Device

The rotation of the hinge connector ψ_y calculated from (21) can be used to compute the total average generated power P_a of the anti-motion device over the range of wave frequency ω considered in the regular wave by using the following expression

$$P_a = \frac{1}{2}\omega^2 \sum_{i=1}^{R} (B_{PTO})_i \left(\psi_y^2\right)_i \tag{22}$$

The total average generated power P_a is then expressed as capture width (CW) [29] by normalising with the wave power resource $P_{resource}$ (24) in order to quantify the efficiency of the anti-motion device in generating wave energy.

$$CW = \frac{P_a}{P_{resource}} \tag{23}$$

The CW is the width of a wave crest that contains the same P_a as extracted by a WEC and the CW has to be as large as possible for the anti-motion device to be effective in generating wave energy. The wave power resource $P_{resource}$ in (23) is given as [30]

$$P_{resource} = \frac{\rho g^2 T H^2}{64\pi} \tag{24}$$

where ρ is the density of sea water, g the gravitational acceleration, T the wave period and H the significant wave height.

3.6 Seeking Optimal B_{PTO} using GA Optimization Scheme

The optimal constant and variable PTO damping for the pontoon-type WEC are sought by using an in-house GA optimization code developed in MATLAB®. The objective function is to achieve maximum absorbed power P_a (22) or CW (23) which indicates the maximum power absorption from the waves. The variables used to satisfy the objective function are the PTO damping B_{PTO} ranging from 0 MN.s/m to $66\frac{2}{3}$ MN.s/m with 40 intervals, hence considering a possibility of 41 PTO damping values for each PTO system. Note that the maximum range of the variables (B_{PTO}) is set to $66\frac{2}{3}$ MN.s/m in the optimization process as the effect of the B_{PTO} on the hydroelastic response becomes negligible when the value is very large. It is noted that the maximum value of $66\frac{2}{3}$ MN.s/m is obtained by normalizing the maximum B_{PTO} of 20 GMN.s by the structural length L of 300 m.

Without the GA optimisation scheme, the total possible combination of the B_{PTO} is denoted by N_T, where N_T is given as

$$N_T = \left(\frac{(B_{PTO})_{max} - (B_{PTO})_{min}}{(B_{PTO})_{interval}} + 1 \right)^{N_L} \tag{25}$$

where N_L is the number of PTO considered in the pontoon-type WEC, i.e. $N_L = R = 99$. Equation (25) will produce a total of 41^{99} possible combinations of PTO damping for the considered WEC, which is obviously impractical due to its large computational cost involved. In order to devise a more practical optimization process, the B_{PTO} along the $y-$axis direction is varied but kept constant along the $x-$axis direction, thus reducing N_L in (25) to 11 for the pontoon-type WEC considered here. The assumption made here is practical from the engineering point of view, as having a constant B_{PTO} along the $y-$axis direction, i.e. along the line hinge, will result in symmetrical structural deflection about the $x-$axis under head sea condition, thus inducing lower stress resultants as compared to its asymmetrical counterpart. Besides, having a uniform B_{PTO} value along the hinge is more practical as it will ease the installation of the PTO system. With $N_L = 11$, N_T is reduced to $41^{11} \approx 5.5 \times 10^{17}$ but is still computationally expensive without the GA optimization scheme.

In order to reduce the computational time to seek for the optimal B_{PTO}, the GA optimization scheme is utilized where it is divided into two steps as depicted in Fig. 4, i.e.

(i) Step 1: Generating an initial population of N_R
(ii) Step 2: Applying GA optimization scheme to the initial population to seek for the optimal B_{PTO}

In Step 1, the initial population of $N_R = 500{,}000$ different combination of B_{PTO} is generated by using a bias distribution. In Step 2, N_I individuals having the highest fitness values in terms of the P_a or CW are then selected from the generated N_R by using the roulette wheel sampling technique [31]. Next, N_I sets of parents (father and mother) are randomly selected from the N_I individuals for the crossover and mutation operations in order to create N_I offspring for the next generation. In addition, the individual with the best fitness value in the current generation are kept for the next generation, and this individual is known as the elite child. This process of crossover, mutation and elitism will continue until the objective function is met, i.e. the maximum P_a or CW has converged. The convergence criteria for the maximum P_a or CW is 0.01%. It is to be noted that although increasing N_I increases the computational time, it ensures a faster computational time in achieving convergence for the P_a or CW, vice-versa. For the case study, $N_I = 50$ is selected as this number is sufficient to ensure a faster convergence based on the authors' computational resource. It is also noted here that the parent are known as the DNA whereas the R numbers of B_{PTO} are known as the chromosomes in the GA optimization scheme.

The chromosomes will be converted into binary numbers of 20 bits for the crossover and mutation processes. The crossover C_c and mutation C_m probabilities are taken as 0.2 and 1.0, respectively. This implies that the crossover process between the two DNAs applies only to 20% of the chromosomes whereas the mutation process only applies to all the chromosome of the best fit. The choice of $C_m = 1.0$ will be explained in Section 4.2.

4. Validation of Results

4.1 Hydroelastic response for interconnected structure

The solver for the equation of motion for the water-plate model (20) is developed in MATLAB®. The code for the hydroelastic analysis is validated with the results of the VLFS presented by Yago and Endo [32] and Fu *et al*. [33] in the subsequent sections.

4.1.1 Convergence Study

A convergence study is performed to investigate the effects of the boundary discretisation on the convergence of the hydroelastic response of the VLFS presented in [33]. The details of the numerical model used are presented in Table 2 and the compliance χ of the hydroelastic response is defined as

$$\chi = \frac{1}{\rho g A^2 BL} \int_{-L/2}^{L/2} \int_{-B/2}^{B/2} |p| \cdot |w| \, dy \, dx \tag{26}$$

The number of elements per wavelength is used as the basis for the discretisation of the plate system. In the present convergence study, the number of elements per wavelength ϵ is taken as 10, 15, 20, and 25; and the number of plate natural modes N_m is taken as 10, 15, 20, and 25. The results are summarized in Table 3 which shows that the compliance of the two-floating plate system for several combination of ϵ and N_m.

As can be seen in Table 3, the compliance χ converges when $\epsilon = 25$ and $N_m = 20$. It is noted that the convergence criteria is 1.5% for ϵ and 1.0% for N_m. Therefore, ϵ = 25 and $N_m = 20$ are considered as the optimal combination of the two parameters for all wavelengths considered, and will be used in the subsequent analyses.

4.1.2 Comparison with Existing Results

The validity and accuracy of the present method for solving the floating plate problem with mechanical line joints is established by comparing the hydroelastic responses computed by the present method with the experimental results obtained by Yago and Endo [32] and the numerical results by Fu *et al*. [33]. The input data for the floating plate problem used by the aforementioned researchers are given in Table 2 where the VLFS considered is a two 150-meter long interconnected floating modules connected by using a mechanical line hinge to form a VLFS with 300m in total length.

The comparison of the hydroelastic response along the centerline of the VLFS between the present numerical results with those found in [32] and [33] are presented in Fig. 5. The good agreement between experimental and numerical results for the continuous structure validates the correctness and accuracy of the present method for evaluating the hydroelastic response of the VLFS with line connectors. The numerical results of the hinged-connected VLFS also show good agreement between the present method and those published in [33].

4.2 GA Optimization Scheme

In order to validate the reliability of the present GA optimization scheme, the results obtained from the GA optimization scheme is compared with their counterparts obtained from the parametric analysis. As the pontoon-type WECs presented in Table 1 are too large to run on the parametric analysis, a much simpler pontoon-type WEC is considered in the validation exercise where the WEC is connected by only a one-line hinge connector with PTO attached to it. The length L and breadth B of the pontoon WEC are taken as 300 m and 60 m, respectively (i.e. Group III in Table 1). Two wave periods are considered here, i.e. $T = 6.2026\ s$ and $T = 8.7668$ s, which corresponds to $\lambda/L = 0.2$ and 0.4, respectively. In the parametric analysis, the B_{PTO} is assumed to range from 0 to $1{,}666\frac{2}{3}$ MN.s/m with an interval of $\frac{1}{300}$ MN.s/m, hence requires an execution of $N_T = 500{,}000$ operations. It is noted that the normalized maximum $B_{PTO} = 1{,}666\frac{2}{3}$ MN. s/m when multiplied with the length $L = 300$ m yields a maximum B_{PTO} of 500 GN. s at each line connector. The B_{PTO} that produces the highest absorbed power P_a or capture width ratio CW is taken as the optimal PTO damping.

On the other hand, the GA optimization scheme is used to obtain the optimal damping following the two steps given in the Section 3.6. In step 1, the initial population N_R is taken as 1% of the N_T, i.e. $N_R = 5{,}000$. These 5,000 initial populated samples are then fed into the GA optimization scheme to obtain the optimal B_{PTO}.

The computational time for both the parametric analysis and GA optimization scheme is compared in Table 4. It can be clearly seen that the number of simulations required for the GA optimization scheme is far lesser than its counterpart for the parametric analysis. As a result, the computational time for the GA optimization scheme is 87.5% faster than the parametric analysis, when running on an Intel® Core™ i7-5600U CPU@2.60Ghz machine. This presents a significant enhancement in the computation time by using the GA optimization scheme and will be useful for larger N_T as presented in the following sections. It is to be noted that the optimal B_{PTO} obtained from the parametric analysis and the GA optimization scheme are the same (refer to Fig. 6), thus confirming the reliability of the present GA code in seeking the optimal B_{PTO}. The evolution of the B_{PTO} to achieve the maximum absorbed power P_a for both $\lambda/L = 0.2$ and 0.4 are presented in Figs. 6(a) and (b), respectively. The various color tones denote the different absorbed power P_a of the WEC corresponding to the respective B_{PTO} in the y-axis. The P_a in the legends changes in ascending order denoted by the lighter to darker tone. It can be seen that the present GA optimization scheme successfully achieves the optimal B_{PTO} at the 86th and 95th iteration.

In the GA optimization scheme presented in Fig. 4, the crossover and mutation probability have to be set in order to accelerate the convergence of the GA process in obtaining the optimal B_{PTO}. Therefore, a convergence test is conducted in Fig. 7 for the same pontoon-type WEC considered in the validation exercise for two different C_m, i.e. $C_m = 0.5$ and $C_m = 1.0$. As can be seen clearly, the GA optimization scheme running at $C_m = 1.0$ accelerates the convergence process in seeking the optimal B_{PTO}. It is noted that $C_m = 1.0$ implies that all the chromosome (i.e. B_{PTO}) is selected to be mutated at each iteration in the GA scheme.

5. Results and Discussion

5.1 Effect of Hydroelastic Response

Figures 8 to 10 show the CW of Groups I ($L = 100$ m), Group II ($L = 200$ m) and Group III ($L = 300$ m) pontoon-type WEC, respectively. Six different Young's moduli, i.e. $E = 0.2, 2, 20, 200, 2000, 20000$ GPa with a constant $B_{PTO} = 600$ kN.s/m are considered. The pontoon-type WEC is subjected to wave frequencies ω ranging from 0.1 rad/s to 1.6 rad/s with wave approaching from the headsea. Figure 8 shows that the 100-m pontoon-type WEC is very effective in generating wave energy when it is connected with the most number of hinges (Type-A). This results in shorter modules rotating in rigid body motion and thus generating more energy when subjected to wave action. Also, the CW or the P_a do not change with respect to the varying structural flexural stiffness, which depends on the Young's modulus E. However, when the pontoon-type WEC gets longer as presented in Figs. 9 and 10, i.e. $L = 200$ m and 300 m, respectively, it can be seen that greater energy can be generated depending on the Young's modulus E of the pontoon-type WEC. It is observed that more energy can be generated by the WEC when each module in the pontoon-type WEC deforms flexibly, with the most energy generated when the module is the most flexible (i.e. $E = 0.2$ GPa). In addition, it is interesting to find out that the amount of energy being generated increases with the reduction in the number of hinges in the WEC. This is because a reduced number of hinges results in longer connected modules, and thus the structures deform in a flexible manner under wave action. As a consequence, the 200-meter and 300-meter long pontoon-type WEC have the highest power generation when the WEC is connected by only one hinge with $E = 0.2$ GPa.

The comparisons of the hydroelastic response of the Group I pontoon-type WEC for different numbers of hinges, i.e. Type-A: 11 hinges, Type-B: 5 hinges, Type-C: 3 hinges and Type-D: no hinges are presented in Figure 11. The deflection is measured along the centerline of the WEC and the structure is subjected to a headsea condition. In each subfigure, the six different lines represent the hydroelastic responses of the WEC with

different E when subjected to their corresponding wave periods T that produce the maximum CW. It can be seen that the influence of the Young's modulus is negligibly small for the WEC connected by large numbers of connectors, i.e. Type-A and Type-B; but its effect increases when the pontoon-type WEC is connected by smaller numbers of module, i.e. Type-C and Type-D. It is also observed clearly that the CW for a continuous pontoon-type WEC (Type-D) is able to generate more energy than its counterpart with connectors. This finding denotes that a significant cost saving could be achieved due to the shorter installation time and the smaller number of connectors needed. In addition, it also saves on material cost as the WEC could be manufactured with lesser material to allow for flexible deformation provided that the stress resultants on the structure are within the stipulated allowable stress limit to ensure the safety and robustness of the structure.

Similarly, the hydroelastic responses for the 200-meter and 300-meter pontoon-type WEC are presented in Figs. 12 and 13, respectively. As the length of the WEC becomes longer, the effect of the Young's modulus E on the motion of the WEC becomes significant. According to Suzuki *et al.*'s [34] definition of a VLFS, the hydroelastic response is only dominant when the following two ratios are larger than 1.0:

i. Structural length/Wavelength (l/λ)
ii. Structural length/Characteristic length (l/λ_c)

The characteristic length λ_c is given as

$$\lambda_c = \sqrt[4]{4\pi^2 \frac{D}{k_c}} \tag{27}$$

where D is the flexural rigidity given as $D = Eh^3/12$ and k_c is the spring constant of the hydrostatic restoring force. By using the ratios given in (i) and (ii) above, this could explain the reason that some of the pontoon-type WECs behave like a rigid body under wave action whereas others in a flexible motion. For example, this can be shown clearly in Fig. 13(d) where the WEC with $E = 20{,}000$ GPa moves in a rigid body motion. Therefore, it is always important to check on these two ratios when designing the pontoon-type WEC.

5.2 Effect of Non-Uniform Optimized PTO Damping

In addition to allowing for certain degree of structural deformation in the pontoon-type WEC, the energy generation from the pontoon-type WEC could be further enhanced by using a non-uniformly distributed optimal PTO damping, termed also as variable PTO system. In order to seek for the optimal PTO damping, the GA optimization scheme as outline in Section 3.6 is used. The Group III ($L = 300$ m) pontoon-type WEC subjected to two different wavelength-to-structural length ratios, i.e. $\lambda/L = 0.2$ and 0.4 is used to demonstrate the power enhancement of the pontoon-type WEC.

By using the GA optimization scheme as given in Section 3.6, with an initial population of $N_R = 500{,}000$, $C_c = 0.2$ and $C_m = 1.0$, the evolution of B_{PTO} for Group III pontoon-type WEC to achieve the optimal B_{PTO} is plotted in Fig. 14. Each subfigure denoted by Fig. 14(a) to (f) represents the WEC connected by different numbers of connection joints and subjected to regular waves of two different λ/L. The optimal damping value at each PTO system that results in the maximum CW is presented in each subfigure. It can be seen that by using the GA optimization scheme, the optimal non-uniform distributed PTO damping at each line connector that produces the maximum power could be obtained. Figure 14 shows that a combination of the minimum B_{PTO} (i.e. 0 MN.s/m) and maximum B_{PTO} (i.e. $66\frac{2}{3}$ MN.s/m) for the pontoon-type WEC could be used to achieve the maximum CW. However, the non-uniform distributed optimal B_{PTO} could be in the range between these minima and maxima values such as for the Type-A pontoon-type WEC, where the WEC is connected by more connection joints.

By focusing on the pontoon-type WEC of Group III Type-A, the evolution of the B_{PTO} is presented in Fig. 15 for four different λ/L, i.e. $\lambda/L = 0.2, 0.4, 0.6$ and 0.8. It can be seen from Fig. 15(a) that the maximum CW can be achieved by using a different combination of B_{PTO} where the optimal B_{PTO} for each PTO system does not necessary be the minimum B_{PTO} (0 MN.s/m) or maximum B_{PTO} ($66\frac{2}{3}$ MN.s/m) considered in Table 1. Figure 15 also shows that the optimal B_{PTO} value could be a combination of the minimum and maximum B_{PTO} to achieve the maximum power generation when the WEC is subjected to large wavelength.

In order to visualize the hydroelastic response of the pontoon-type WEC under uniform and non-uniform optimal B_{PTO}, the deflection along the centerline of the WEC is plotted in Fig. 16 for the Group III Types-A to -C pontoon-type WEC. A comparison of the deflection is made between the WEC connected by variable PTO system with that by uniform PTO system. It can be seen clearly from Fig. 16 that the CW of the non-uniform optimal B_{PTO} counterpart is greater than that predicted by the uniform

counterpart. However, the difference is more obvious for Type-A pontoon-type WEC due to the greater magnitude of rotational motion in the WEC. Similarly, the same results are plotted for $\lambda/L = 0.4, 0.6$ and 0.8 in Figs. 17 to 19, respectively, and similar observation can be made on the CW of the WEC. An interesting point to make when comparing the results presented in Figs. 16 to 19 is that the difference of the CW for the WEC connected by variable PTO system with its uniform counterpart becomes greater when the wavelength increases. This suggests that the optimal variable PTO system is more effective when the WEC is subjected to regular waves of longer wavelengths due to the larger magnitude of hydroelastic response. In addition, the CW for the WEC is found to increase with the increase in wavelength.

In Figure 20, a comparison of the hydroelastic response of the pontoon-type WEC with Types-A, -B and -C pontoon-type WEC with the continuous pontoon-type WEC (Type-D) is presented. These WECs are subjected to four different λ/L ranging from 0.2 to 0.8, with an interval of 0.2. It is interesting to note that the continuous pontoon-type WEC is the most effective among the four in generating wave energy when it is equipped with optimal variable PTO system. The optimal B_{PTO} obtained from the GA optimization scheme in this case falls in the higher range of the B_{PTO} considered in Table 1 to achieve the maximum CW.

6. Conclusion

The pontoon-type WEC was considered and the coupled finite element-boundary element method was used to solve for the hydroelastic response of the WEC. The GA optimization scheme was utilized in seeking the optimal PTO damping of the variable PTO system, where the objective function was to achieve a maximum capture width CW or the absorbed power P_a of the WEC. Three WEC lengths were considered, i.e. $L = 100$ m, 200 m and 300 m, which were categorized as Group I, II and III, respectively. Four different numbers of interconnected modules, i.e. $N = 12, 6, 3$ and 1 were then considered for each group of WEC, which were termed as Types-A, -B, -C and -D, respectively. The two objectives of the paper were successfully achieved, that is to enhance the power generation of the WEC via certain allowance of structural deformation and installation of variable PTO system.

In the investigation on the effect of structural deformation, i.e. structural rigidity, on the power enhancement of the pontoon-type WEC, it was found that greater energy could be generated when the interconnected module in the WEC is allowed to deform under wave action. The effect of structural deformation is even larger when the structural length increases and when the number of interconnected hinge reduces. It is

interesting to note that a continuous pontoon-type WEC without any hinge connector is able to generate the greatest amount of energy among the cases considered in the study. The effect of Young's modulus was found to be significant when the Group II and III pontoon-type WECs are connected with smaller amount of hinge connectors. This is because lesser number of hinge connectors imply longer interconnected floating modules and thus higher structural deformations under wave action. The results presented show that a significant saving in cost, material and connector installation could be achieved for the pontoon-type WEC and at the same time producing high amount of electricity, provided that the structural integrity of the WEC is preserved.

In the investigation on the effect of utilizing variable PTO system on the power enhancement of pontoon-type WEC, it was found that in some cases, the maximum power generation could be achieved by merely utilizing a combination of minimum and maximum B_{PTO} that were considered in the case study. However, it was also found that the optimal non-uniform B_{PTO} for the Type-A pontoon-type WEC comprises a combination of B_{PTO} that falls in between the minimum and maximum B_{PTO} considered. These optimal B_{PTO} was successfully sought by using the GA optimization scheme. The effect of variable PTO system was found to be significant with the increase in the number of hinge connectors and wavelengths. This is due to the greater magnitude of rotational motion in the WEC.

In summary, it was proven from the study that the power generation of the pontoon-type WEC can be enhanced by allowing the structure to deform flexibly under wave action as well as by installing a series of variable PTO system in the pontoon-type WEC. This outcome will be useful to academia and industry working on achieving the power enhancement of WEC.

7. References

[1] Clément, A, McCullen, P, Falcão, A, Fiorentino, A, Gardner, F, Hammarlund, K, Lemonis, G, Lewis, T, Nielsen, K, Petroncini, S, Pontes, M-T, Schild, P, Sjöström, B-O, Sørensen, HC and Thorpe, T, Wave energy in Europe: current status and perspectives, *Renewable and Sustainable Energy Reviews*, 6 (2002), 405-431.

[2] Mørk, G, Barstow, S, Kabuth, A and Pontes, MT, Assessing the global wave energy potential, *Proceedings of the 29th International Conference on Ocean, Offshore and Arctic Engineering*, Shanghai, China,

[3] Yemm, R, Pizer, D, Retzler, C and Henderson, R, Pelamis: experience from concept to connection, *Philosophical Transactions of the Royal Society of London A: Mathematical, Physical and Engineering Sciences*, 370 (2012), 365-380.

[4] Borgarino, B, Babarit, A and Ferrant, P, Impact of wave interactions effects on energy absorption in large arrays of wave energy converters, *Ocean Engineering*, 41 (2012), 79-88.
[5] Sarkar, D, Renzi, E and Dias, F, Wave farm modelling of oscillating wave surge converters, *Proceedings of the Royal Society A: Mathematical, Physical and Engineering Sciences*, 470(2167), (2014), 20140118.
[6] Tay, ZY and Venugopal, V, Hydrodynamic interactions of oscillating wave surge converters in an array under random sea state, *Ocean Engineering*, 145 (2017), 382-394.
[7] Tay, ZY and Venugopal, V, The impact of energy extraction of wave energy converter arrays on wave climate under multi-directional seas, *Journal of Ocean Engineering and Marine Energy*, (2019), 1-22.
[8] Tay, ZY and Venugopal, V, Optimization of Spacing for Oscillating Wave Surge Converter Arrays Using Genetic Algorithm, *Journal of Waterway, Port, Coastal, and Ocean Engineering*, 143(2), (2016), 04016019.
[9] Noad, IF and Porter, R, Optimisation of arrays of flap-type oscillating wave surge converters, *Applied Ocean Research*, 50 (2015), 237-253.
[10] Wei, Y, Barradas-Berglind, JJ, van Rooij, M, Prins, WA, Jayawardhana, B and Vakis, AI, Investigating the adaptability of the multi-pump multi-piston power take-off system for a novel wave energy converter, *Renewable Energy*, 111 (2017), 598-610.
[11] De Backer, G, Vantorre, M, Beels, C, De Rouck, J and Frigaard, P, Power absorption by closely spaced point absorbers in constrained conditions, *IET Renewable Power Generation*, 4 (2010), 579-591.
[12] Haren, P and Mei, CC, An array of Hagen-Cockerell wave power absorbers in head seas, *Applied Ocean Research*, 4 (1982), 51-56.
[13] Alam, M-R, Nonlinear analysis of an actuated seafloor-mounted carpet for a high-performance wave energy extraction, *Proceedings of the Royal Society of London A: Mathematical, Physical and Engineering Sciences*, 468 (2012), 3153-3171.
[14] Chaplin, JR, Farley, FJM, Prentice, ME, Rainey, RCT, Rimmer, SJ and Roach, AT, Development of the ANACONDA all-rubber WEC, *Proceedings of the 7th European Wave and Tidal Energy Conference*, Porto, Portugal, 11-13 September 2007,
[15] Jean, P, Wattez, A, Ardoise, G, Melis, C, Van Kessel, R, Fourmon, A, Barrabino, E, Heemskerk, J and Queau, J, Standing wave tube electro active polymer wave energy converter, *Electroactive Polymer Actuators and Devices (EAPAD) 2012*, 83400C.
[16] Algie, C, Ryan, S and Fleming, A, Predicted power performance of a submerged membrane pressure-differential wave energy converter, *International Journal of Marine Energy*, 20 (2017), 125-134.
[17] Zhang, X, Lu, D, Guo, F, Gao, Y and Sun, Y, The maximum wave energy conversion by two interconnected floaters: Effects of structural flexibility, *Applied Ocean Research*, 71 (2018), 34-47.

[18] Philippe Jean, AW, Guillaume Ardoise, C Melis, R Van Kessel, A Fourmon, E Barrabino, J Heemskerk, J P Queau, Standing wave tube electro active polymer wave energy converter, *Proc. SPIE 8340, Electroactive Polymer Actuators and Devices (EAPAD)*, 83400C.

[19] Michailides, C, Power performance and dynamic response of the WLC wave energy converter based on hydroelastic analysis, *International Journal of Marine Energy*, 19 (2017), 83-94.

[20] Zhang, H, Xu, D, Zhao, H, Xia, S and Wu, Y, Energy extraction of wave energy converters embedded in a very large modularized floating platform, *Energy*, 158 (2018), 317-329.

[21] Tay, ZY, Energy extraction from an articulated plate anti-motion device of a very large floating structure under irregular waves, *Renewable Energy*, 130 (2019), 206-222.

[22] Nguyen, HP, Wang, CM, Flocard, F and Pedroso, DM, Extracting energy while reducing hydroelastic responses of VLFS using a modular raft wec-type attachment, *Applied Ocean Research*, 84 (2019), 302-316.

[23] Davis, L, *Handbook of genetic algorithms*, Van Nostrand Reinhold, New York, USA, 1991.

[24] Bean, JC, Genetic algorithms and random keys for sequencing and optimization, *ORSA journal on computing*, 6(2), (1994), 154-160.

[25] Faltinsen, O, *Sea loads on ships and offshore structures*, Cambridge university press1993.

[26] Wang, CM and Tay, ZY, Hydroelastic analysis and response of pontoon-type very large floating structures, *Fluid structure interaction II*, Springer2011, pp. 103-130.

[27] Tay, ZY, Wang, CD and Wang, CM, Hydroelastic response of a box-like floating fuel storage module modeled using non-conforming quadratic-serendipity Mindlin plate element, *Engineering Structures*, 29(12), (2007), 3503-3514.

[28] Tay, ZY, Wang, CM and Utsunomiya, T, Hydroelastic responses and interactions of floating fuel storage modules placed side-by-side with floating breakwaters, *Marine Structures*, 22(3), (2009), 633-658.

[29] Babarit, A and Hals, J, On the maximum and actual capture width ratio of wave energy converters, *Proceedings of the 10th European Wave Energy Conference*,

[30] Goda, Y, *Random Seas and Design of Maritime Structures*, World Scientific Publishing Company2010.

[31] Goldberg, DE and Deb, K, A comparative analysis of selection schemes used in genetic algorithms, *Foundations of Genetic Algorithms*, Elsevier1991, pp. 69-93.

[32] Yago, K and Endo, H, On the hydoroelastic response of box-shaped floating structure with shallow draft, *Journal of the Society of Naval Architects of Japan*, 1996(180), (1996), 341-352.

[33] Fu, S, Moan, T, Chen, X and Cui, W, Hydroelastic analysis of flexible floating interconnected structures, *Ocean Engineering*, 34(11-12), (2007), 1516-1531.

[34] Suzuki, H, Yasuzawa, Y, Fujikubo, M, Okada, S, Endo, H, Hattori, Y, Okada, H, Watanabe, Y, Morikawa, M and Ozaki, M, Structural response and design of large scale floating structure, *Proceedings of the 1997 16th International Conference on Offshore Mechanics and Arctic Engineering. Part 1-B (of 6)*, Yokohama, Japan, 13-17 April 1997, 131-137.

TABLE 1 – PROPERTIES FOR DIFFERENT CASE STUDIES CONSIDERED

Group	Structural Properties								PTO System	Wave Properties	Water Depth
	$L(m)$	Type	N	E (GPa)	$\rho_p \left(\frac{kg}{m^3}\right)$	$B\ (m)$	$h\ (m)$	$T_w\ (m)$	R	$B_{PTO}\left(\frac{MN\cdot}{m}\right.$	$\omega\left(\frac{rad}{s}\right)$	$H\ (m)$
I	100	A B C D	2	0.2, 2, 20, 200, 2,000 & 20,000	512.5	30	2	1	9	0 to $66\frac{2}{3}$ (5/3 interval)	0.1 to 1.6 (0.025 interval)	600
II	200	A B C D	2									
III	300	A B C D	2									

TABLE 2 – DETAILS OF FLOATING MODEL USED FOR CONVERGENCE STUDY

Parameter	Symbol	Unit	Value
Total length of plate system	L	m	300
Total width of plate system	B	m	60
Total height of plate system	h	m	2
Density of plate system	ρ_p	kg/m^3	256.25
Young's modulus	E	GN/m^2	11.9
Poisson's ratio	ν		0.13
Water depth	H	m	58.5
Wavelength-to-plate length ratio	λ/L		0.2 to 0.8

TABLE 3 – COMPLIANCE FOR SEVERAL COMBINATIONS OF ϵ AND N_m FOR THE NUMERICAL MODEL PRESENTED IN TABLE 1

λ/L	ϵ	N_m			
		10	15	20	25
0.2	10	80.3251	79.2741	79.2671	79.3101
	15	72.5620	71.4070	71.3960	71.4618
	20	70.8723	69.6753	69.6637	69.7332
	25	69.9075	68.6846	68.6725	68.7465
0.3	10	110.1649	108.9089	108.9065	108.9100
	15	107.7885	106.3295	106.3270	106.3681
	20	106.5589	105.0325	105.0293	105.1020
	25	106.0471	104.4847	104.4810	104.5686
0.4	10	158.7024	158.8295	158.7786	158.7543
	15	156.8455	157.1072	157.0976	157.0865
	20	156.3173	156.6538	156.6597	156.6603
	25	156.3556	156.7330	156.7524	156.7664

TABLE 4 – COMPUTATIONAL TIME FOR PARAMETRIC ANALYSIS VS GA OPTIMISATION SCHEME

	Parametric Analysis		GA		Time Reduction in GA (%)
λ/L	No. of simulation	Computational time (hours)	No. of simulation	Computational time (hours)	
0.2	500,000	28	5000 (Step 1*) + 600 (Step 2*)	3.5	87.5
0.4					

*Refer to the steps for GA in Section 3.6

Notes:

1. Optimal B_{PTO} and P_a obtained from both conventional and GA optimization scheme are the same.
2. Please refer to Fig. 6 for the respective B_{PTO} values.

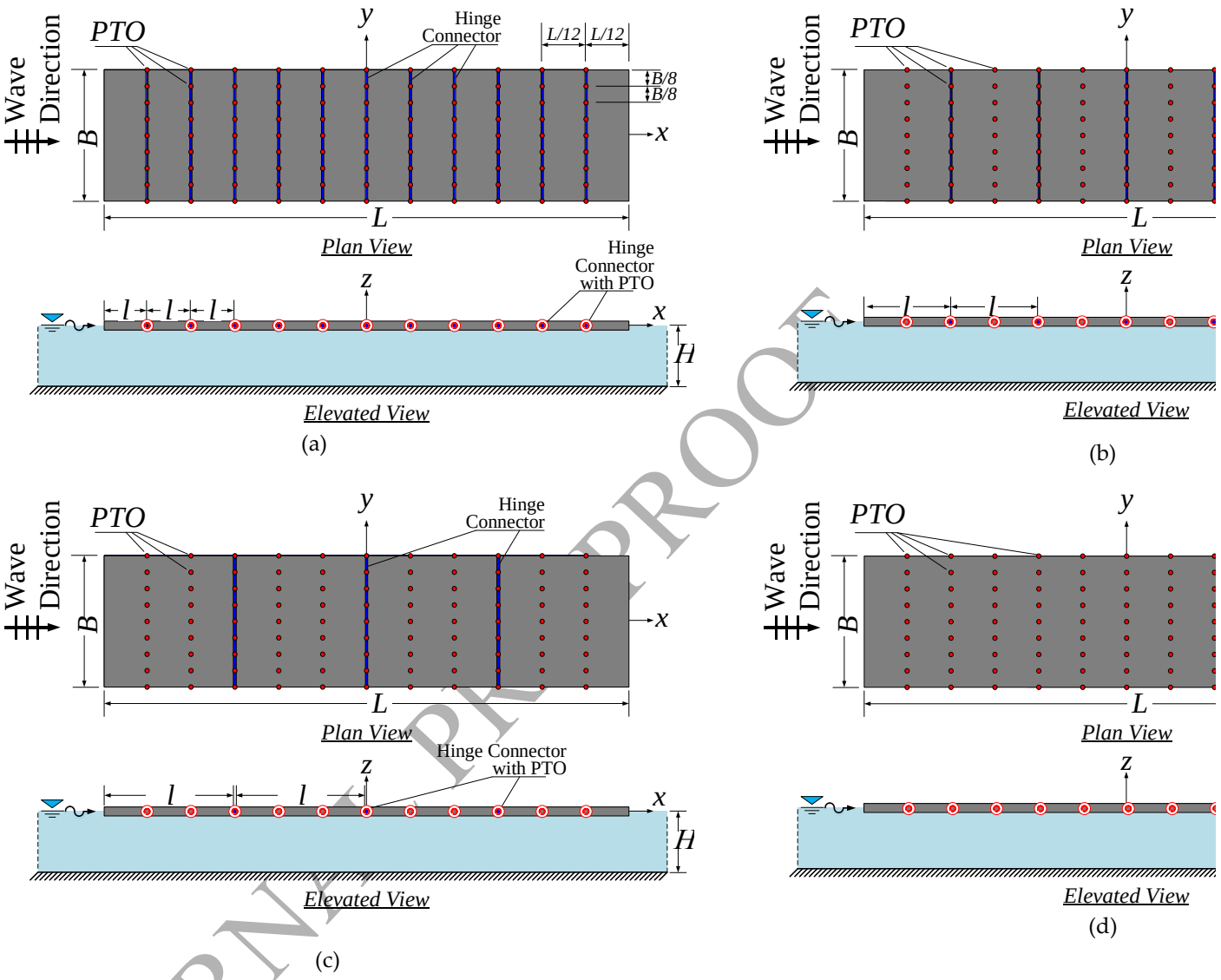

Figure 1 – Pontoon-Type WEC with (a) Type-A: $N = 12$ modules (b) Type-B: $N = 6$ modules (c) Type-C: $N = 4$ modules (d) Type-D: $N = 1$ module

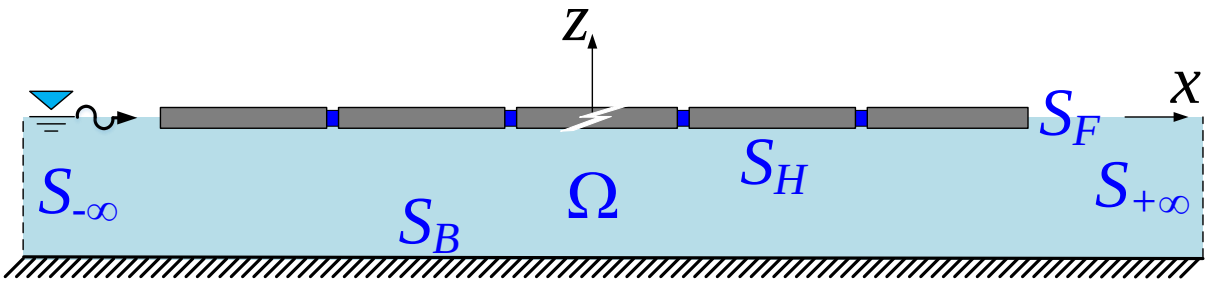

Figure 2 – Computation domain for pontoon-type WEC

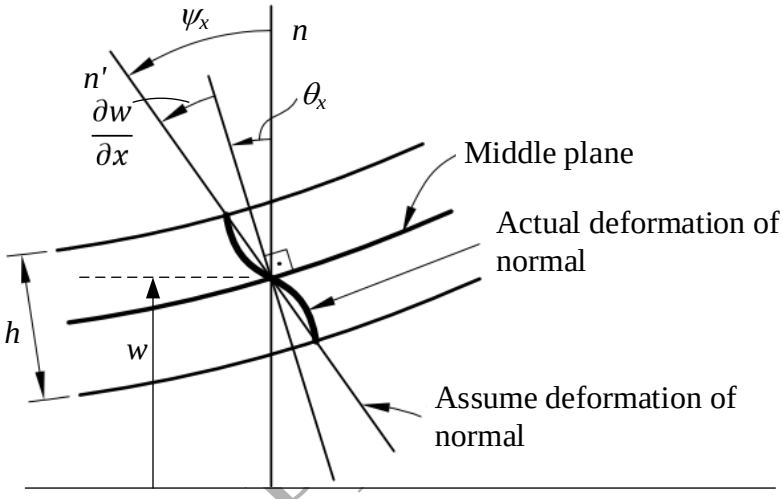

Figure 3 – Figure showing w and ψ_x of Mindlin Plate Theory.

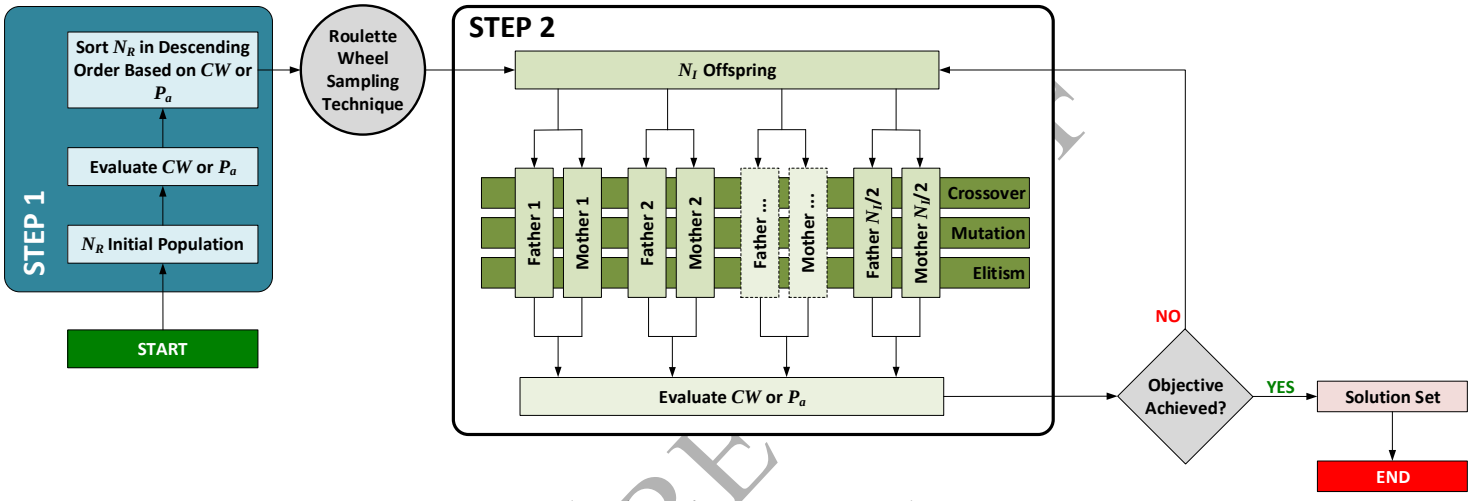

Figure 4 – Flow chart of GA optimization scheme

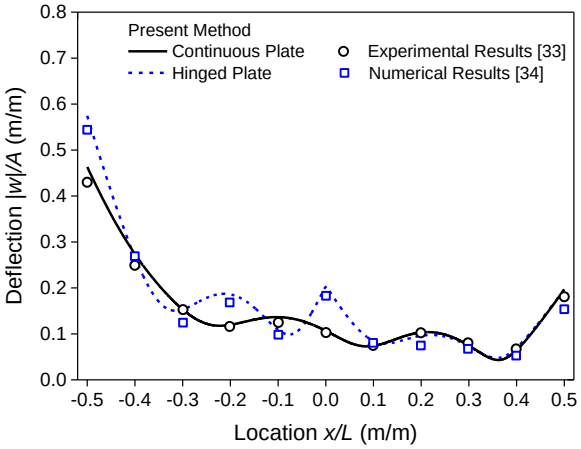

(a)

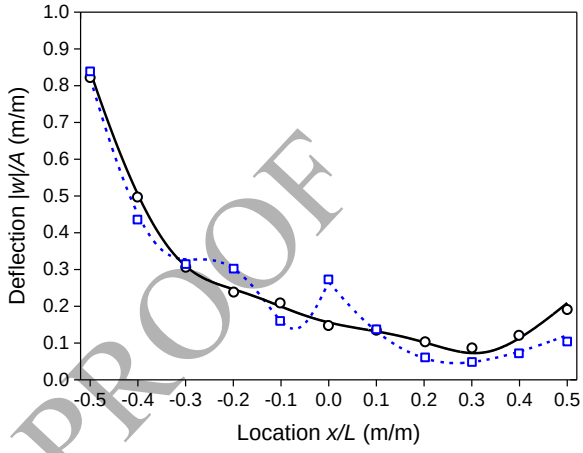

(b)

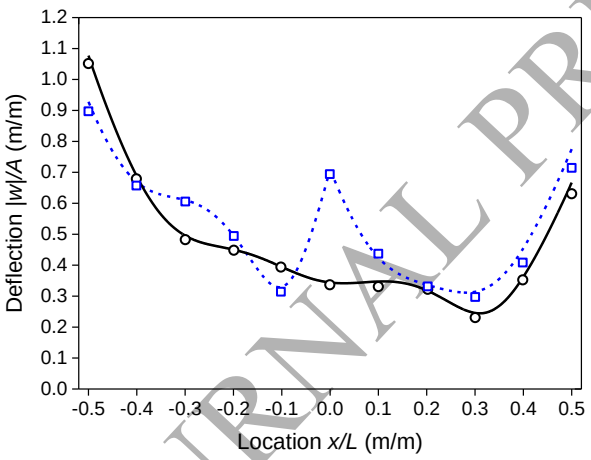

(c)

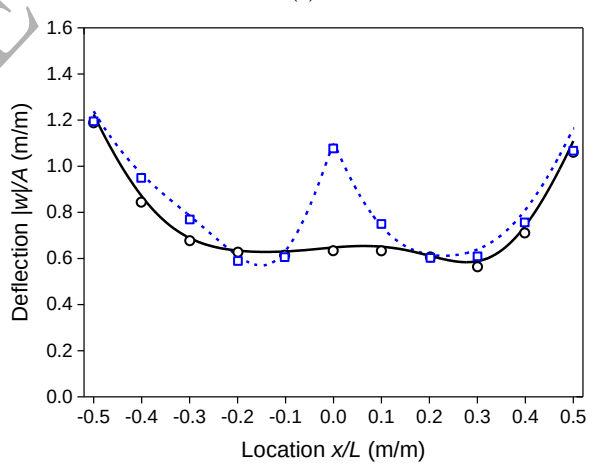

(d)

Figure 5 – Hydroelastic response along the center line of VLFS in Table 2 under (a) $\lambda/L = 0.2$ (b) $\lambda/L = 0.4$ (c) $\lambda/L = 0.6$ (d) $\lambda/L = 0.8$. Headsea condition.

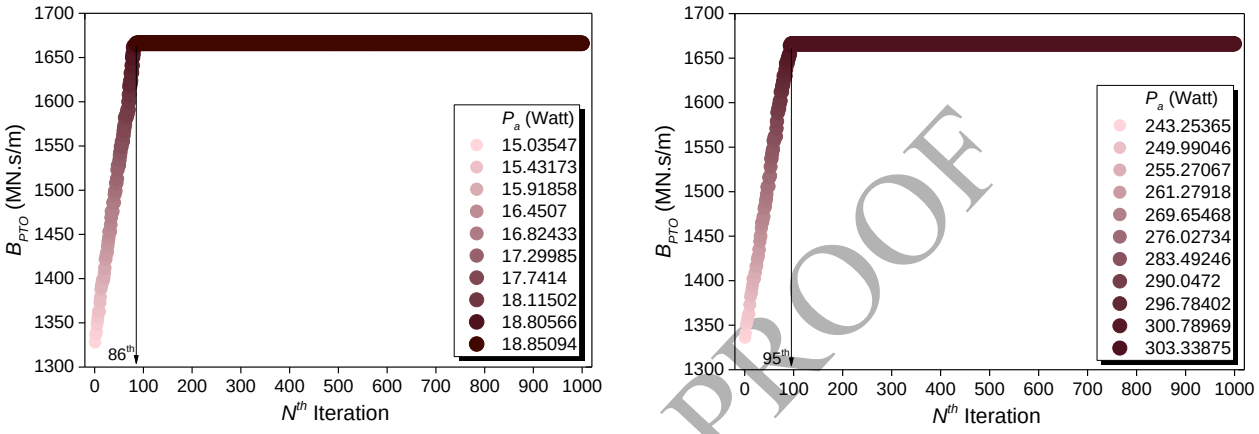

(a) (b)

Figure 6 – Evolution of B_{PTO} to achieve maximum absorbed power P_a using GA optimization scheme for (a) $\lambda/L = 0.2$ and (b) $\lambda/L = 0.4$. $C_m = 1.0$ and $C_s = 0.2$.

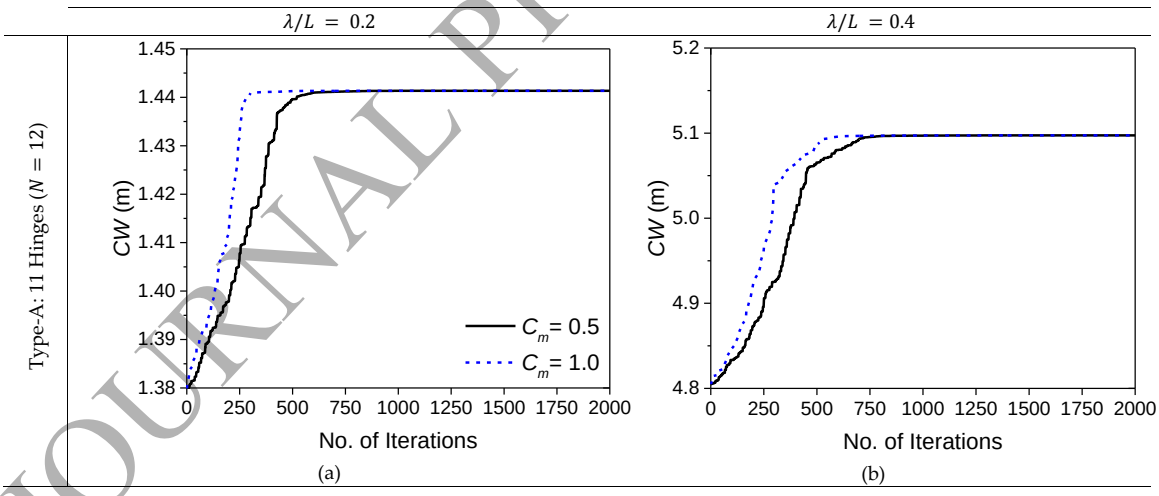

(a) (b)

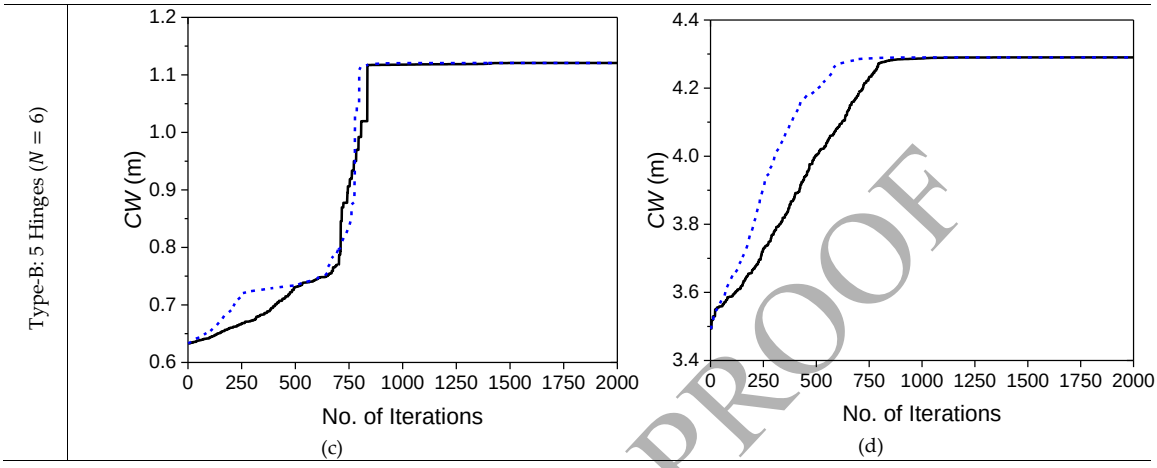

Figure 7 – Convergence test for Group III ($L = 300$) pontoon-type WEC under GA optimization scheme for two different C_m. $C_s = 0.2$.

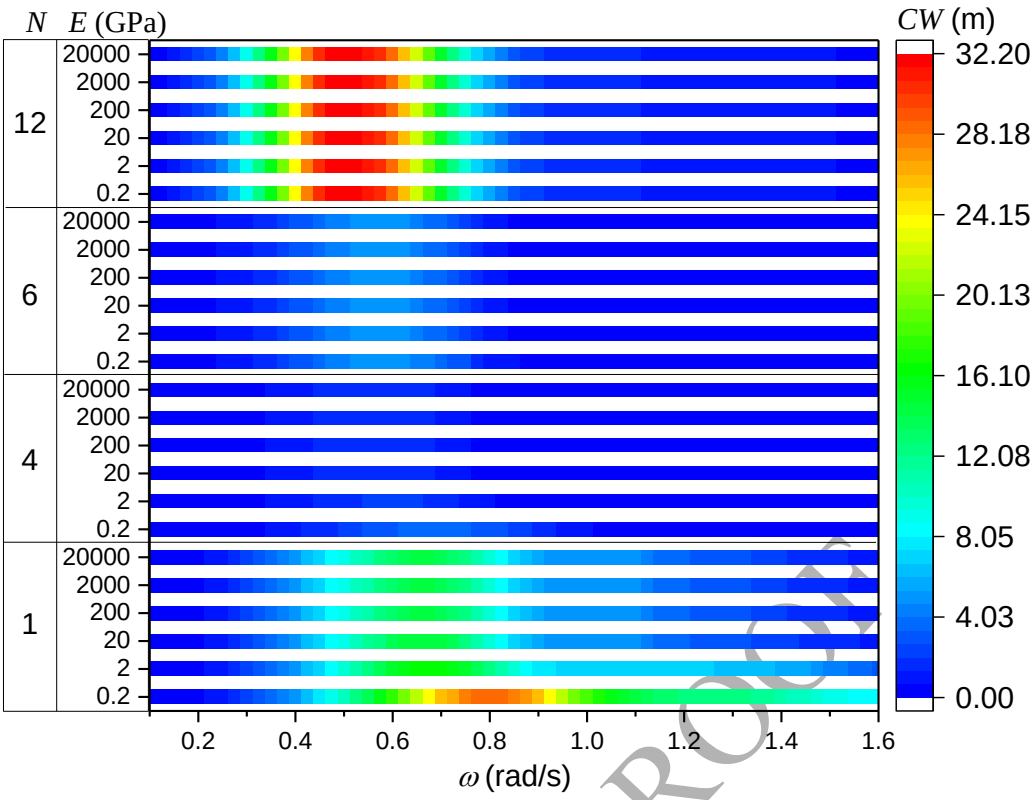

Figure 8 – Capture width CW for Group I Pontoon-type WEC ($L = 100$ m) under different Young's Modulus E

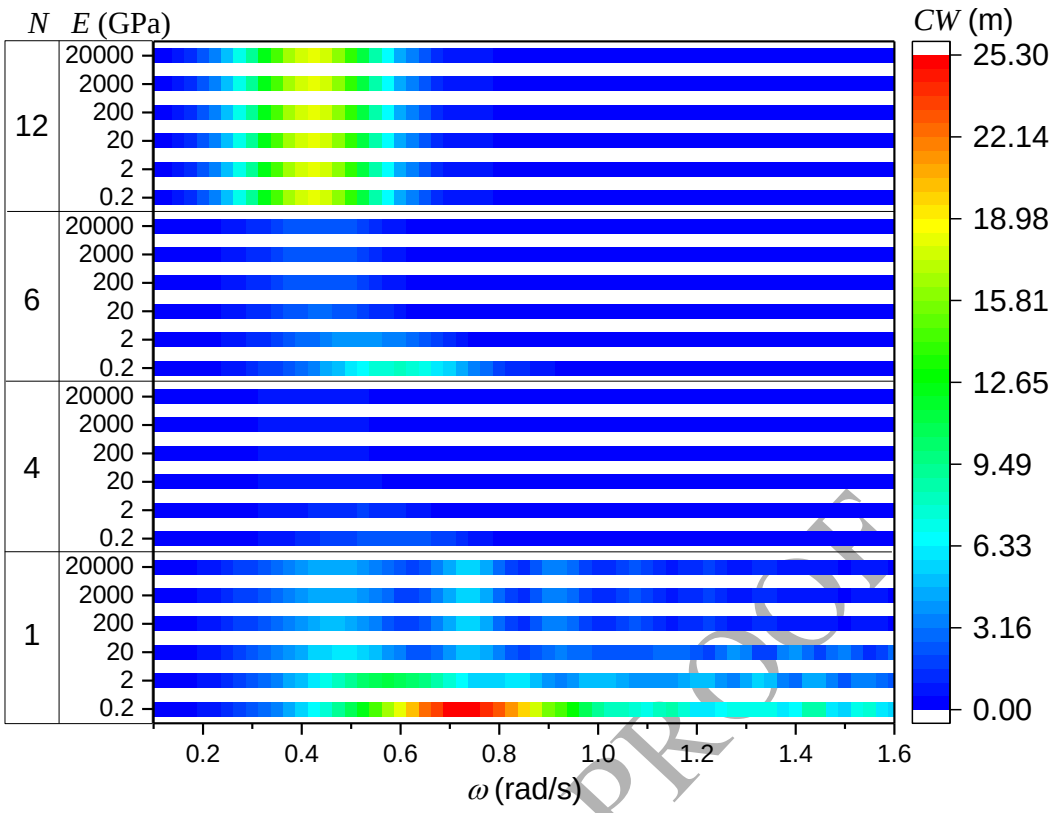

Figure 9 – Capture width CW for Group II Pontoon-type WEC ($L = 200$ m) under different Young's Modulus E

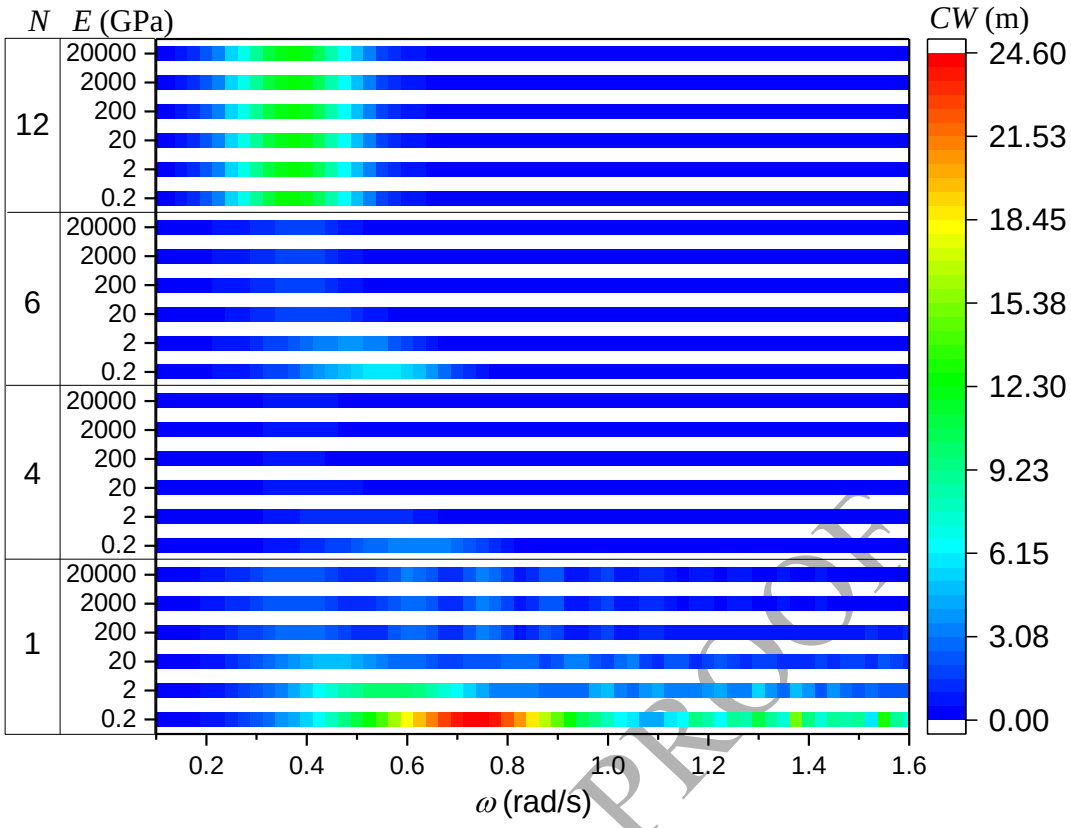

Figure 10 – Capture width CW for Group III Pontoon-type WEC ($L = 300$ m) under different Young's Modulus E

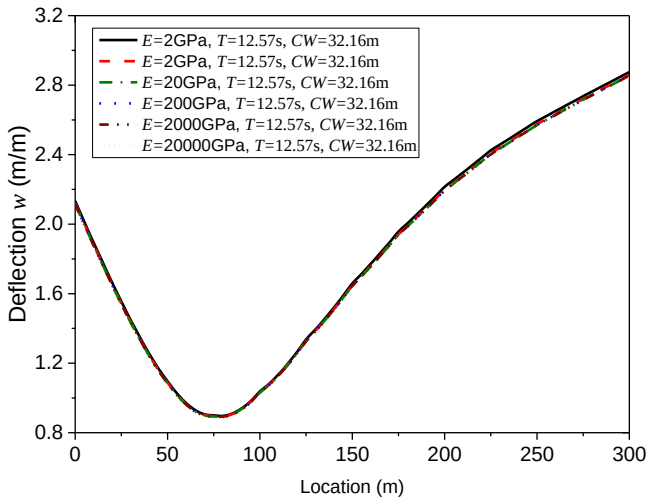

(a)

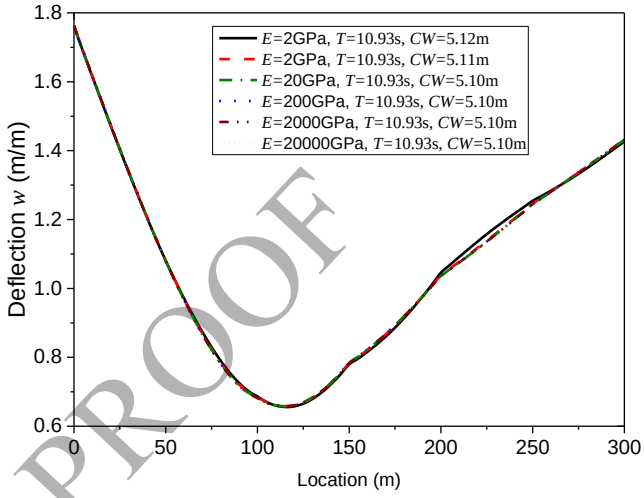

(b)

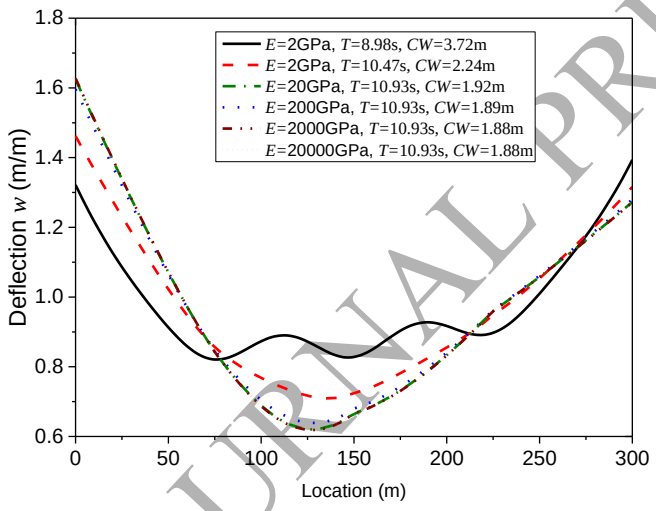

(c)

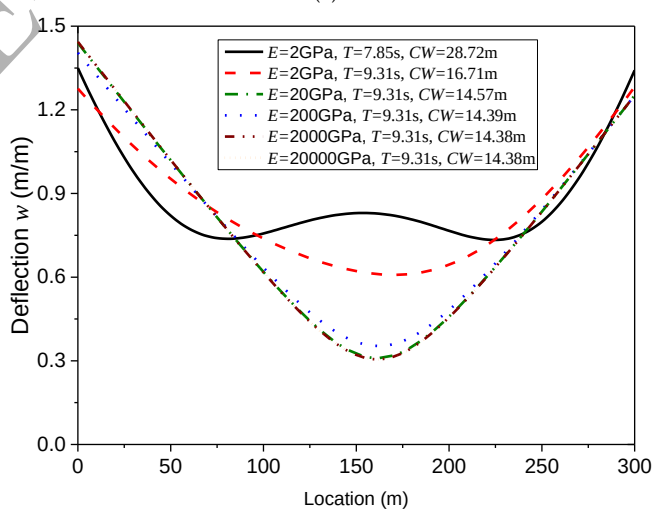

(d)

Figure 11 – Hydroelastic response for Group I ($L = 100$ m) pontoon-type WEC with (a) Type-A: $N = 12$ modules (b) Type-B: $N = 6$ modules (c) Type-C: $N = 4$ modules (d) Type-D: $N = 1$ module

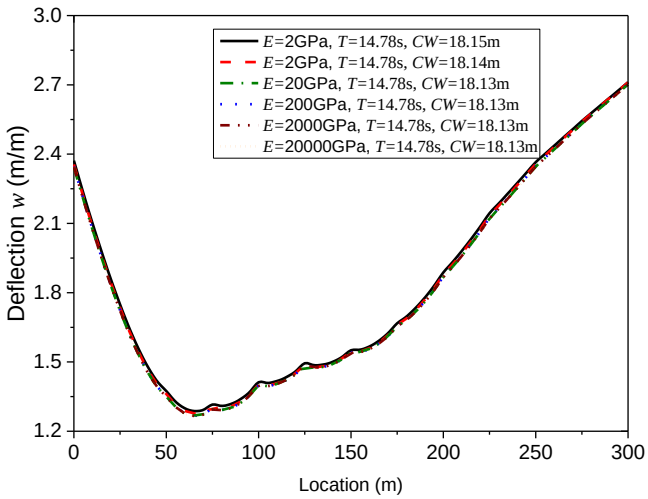

(a)

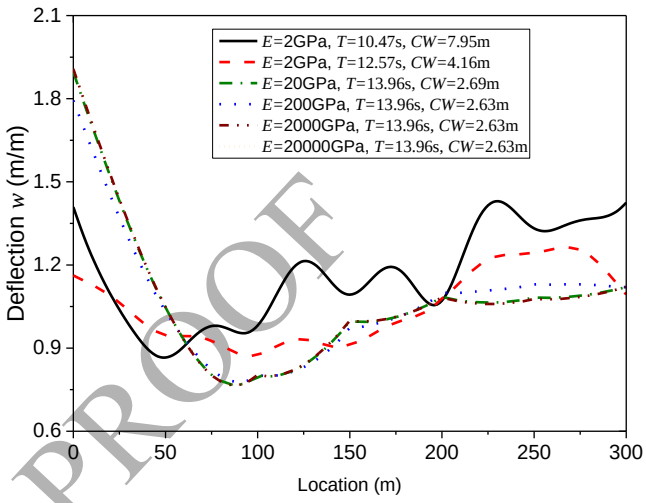

(b)

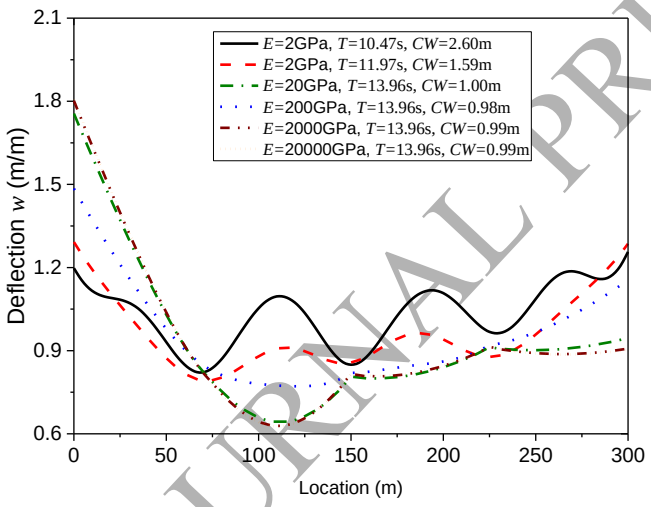

(c)

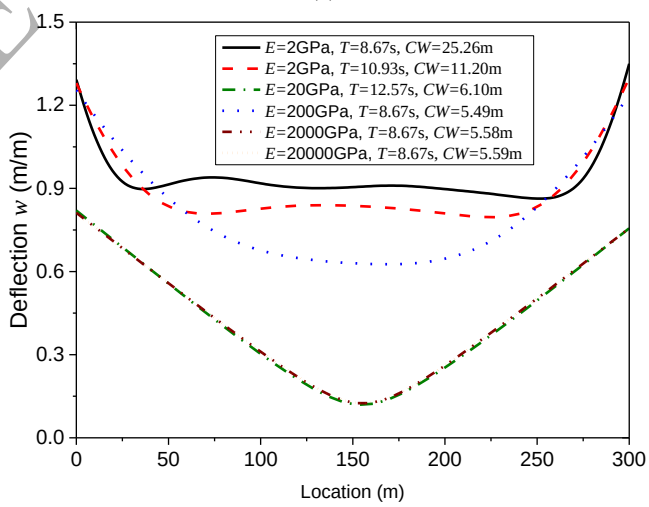

(d)

Figure 12 – Hydroelastic response for Group II ($L = 200$ m) pontoon-type WEC with (a) Type-A: $N = 12$ modules (b) Type-B: $N = 6$ modules (c) Type-C: $N = 4$ modules (d) Type-D: $N = 1$ module

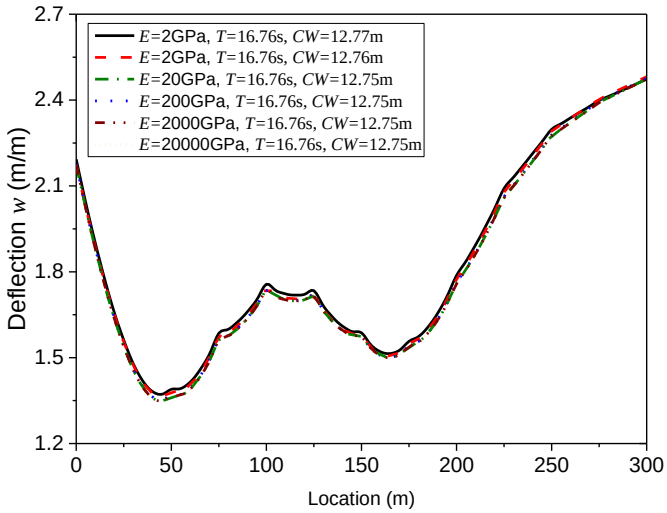

(a)

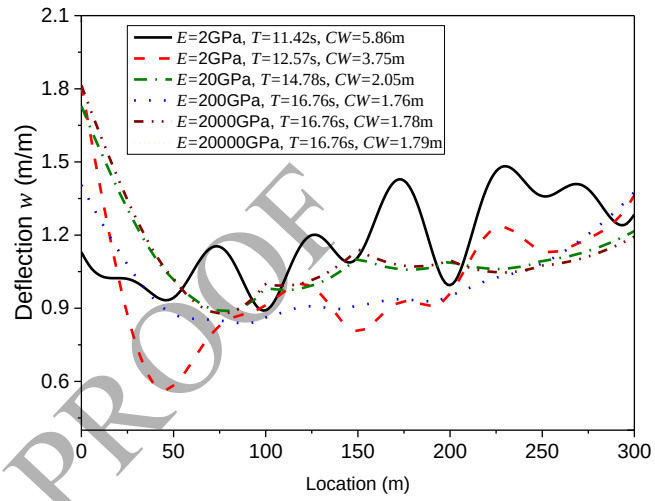

(b)

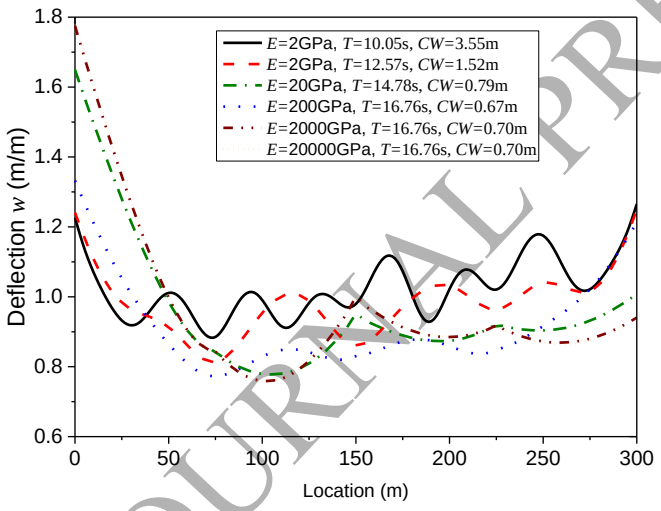

(c)

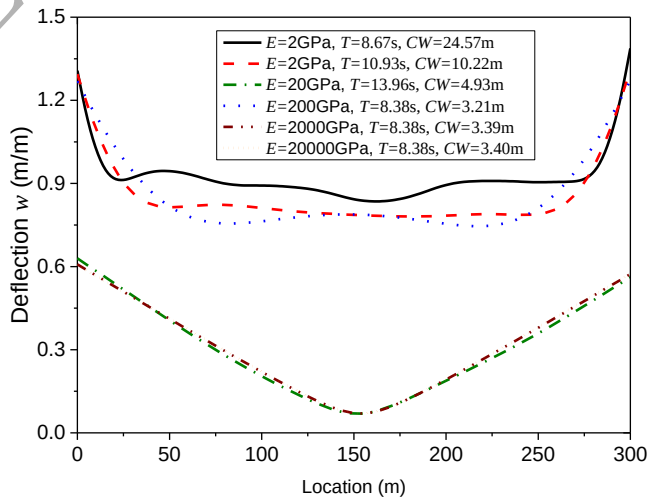

(d)

Figure 13 – Hydroelastic response for Group II ($L = 300$ m) pontoon-type WEC with (a) Type-A: $N = 12$ modules (b) Type-B: $N = 6$ modules (c) Type-C: $N = 4$ modules (d) Type-D: $N = 1$ module

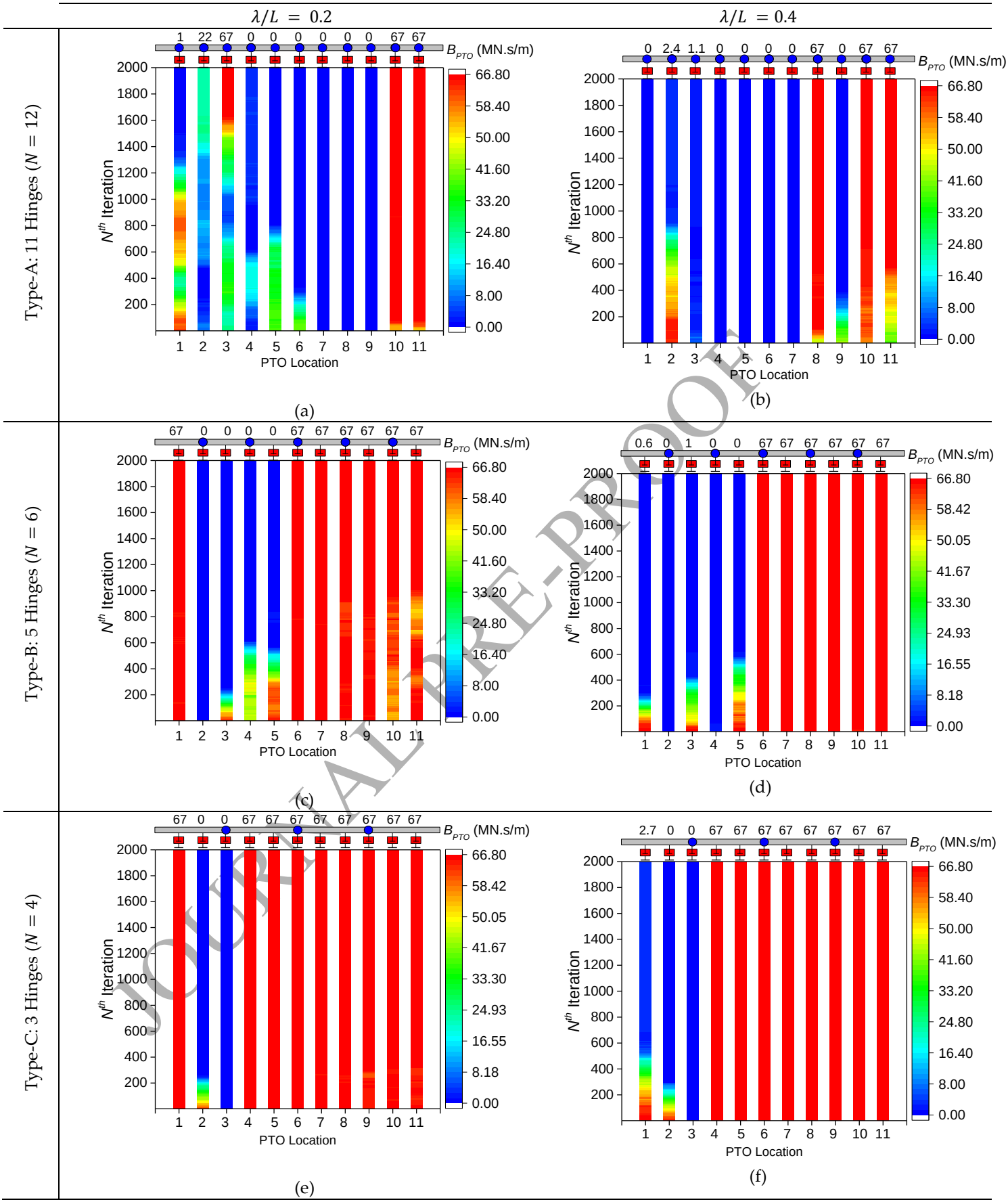

Figure 14 – Evolution of PTO damping B_{PTO} for Group III (L = 300 m) pontoon-type WEC under GA optimization scheme.

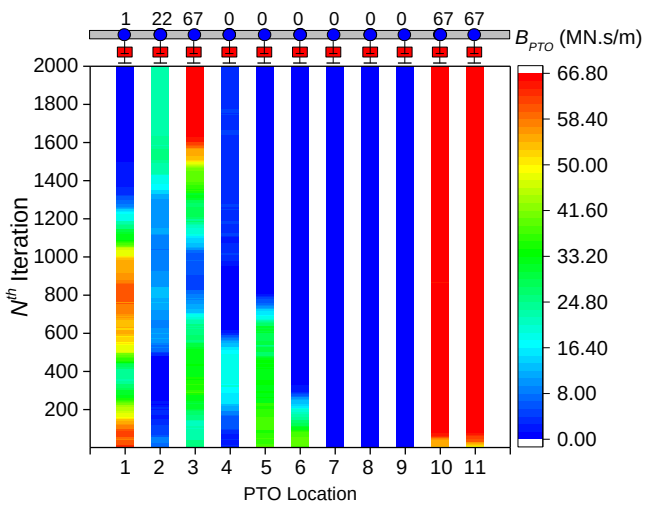

(a) $\lambda/L = 0.2$

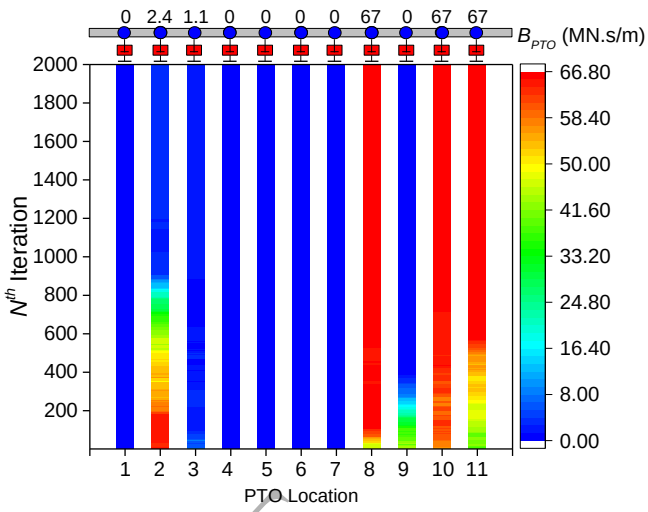

(b) $\lambda/L = 0.4$

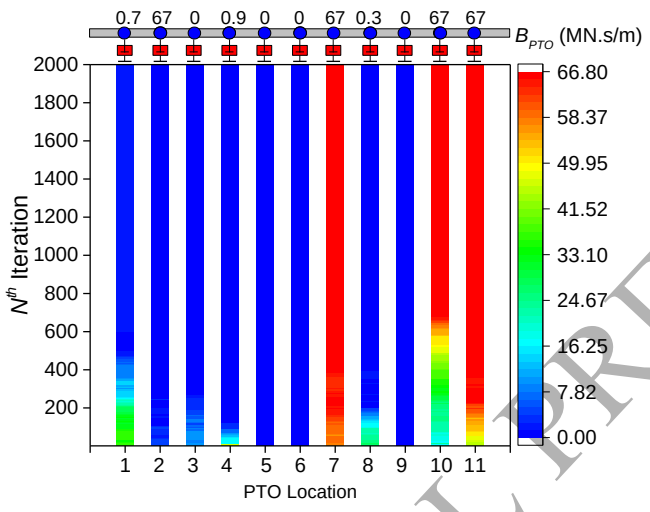

(c) $\lambda/L = 0.6$

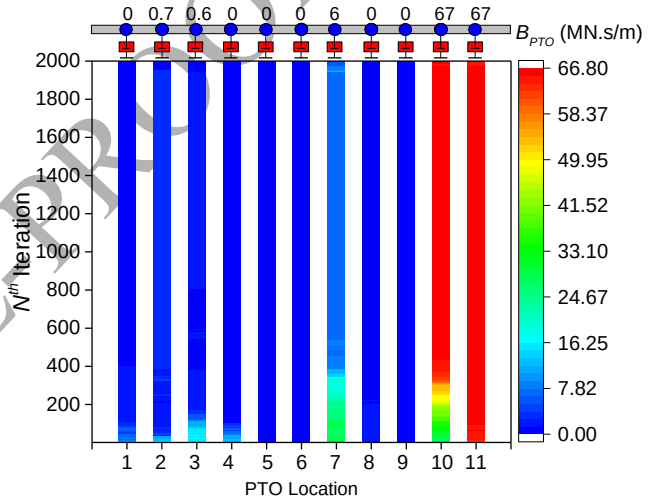

(d) $\lambda/L = 0.8$

Figure 15 – Evolution of PTO damping B_{PTO} for Group III ($L = 300$ m) Type-A ($N = 12$ modules) pontoon-type WEC under GA optimization scheme.

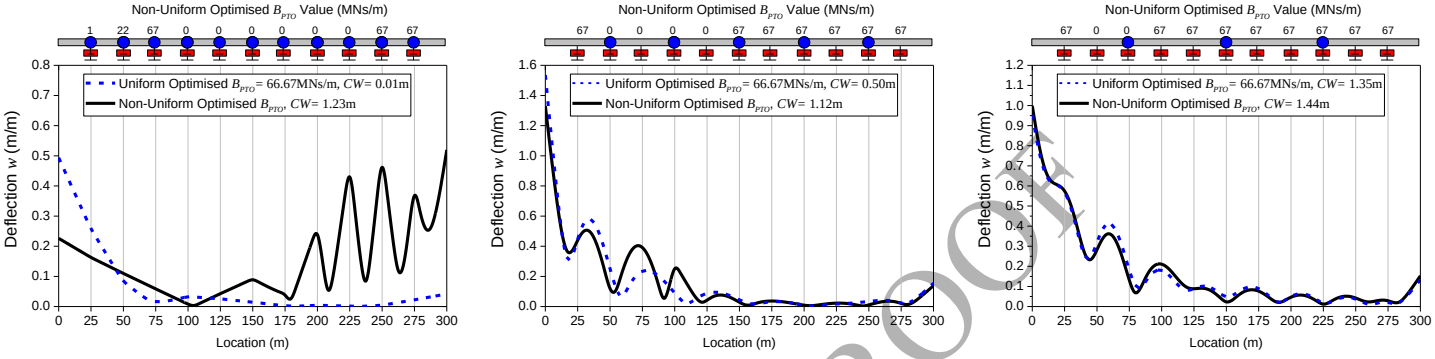

(a) Type-A: $N = 12$ Modules (b) Type-B: $N = 6$ Modules (c) Type-C: $N = 4$ Modules

Figure 16 – Hydroelastic response for Group III pontoon-type WEC under $\lambda/L = 0.2$ with uniform and non-uniform optimized PTO damping

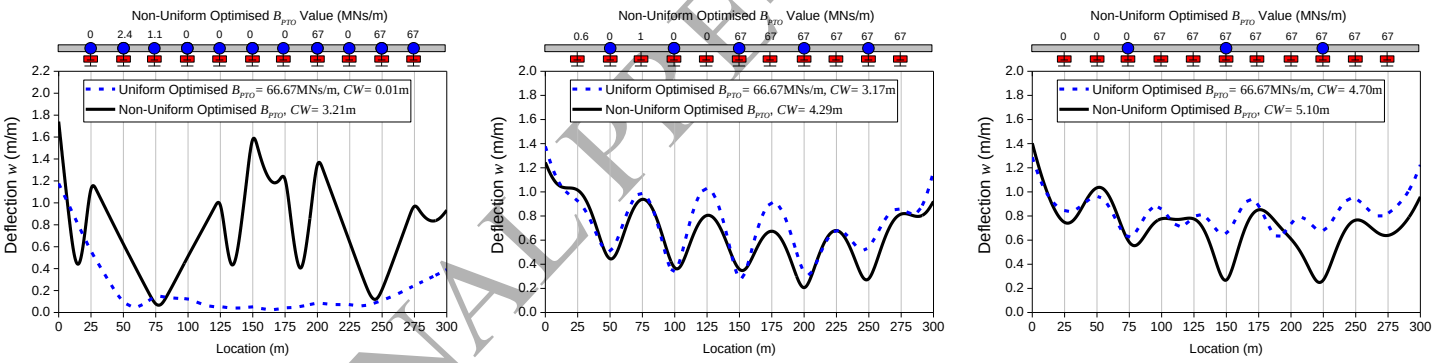

(a) Type-A: $N = 12$ Modules (b) Type-B: $N = 6$ Modules (c) Type-C: $N = 4$ Modules

Figure 17 – Hydroelastic response for Group III pontoon-type WEC under $\lambda/L = 0.4$ with uniform and non-uniform optimized PTO damping

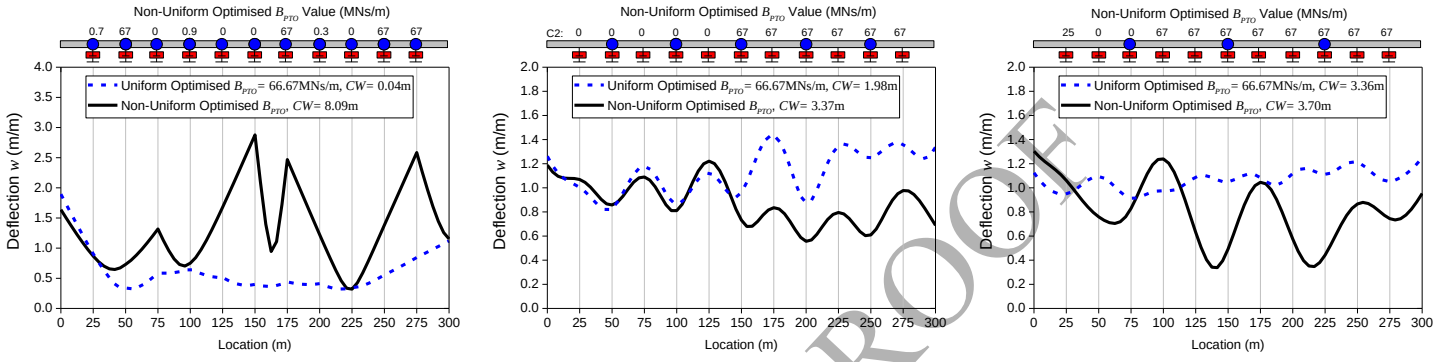

(a) Type-A: $N = 12$ Modules (b) Type-B: $N = 6$ Modules (c) Type-C: $N = 4$ Modules

Figure 18 – Hydroelastic response for Group III pontoon-type WEC under $\lambda/L = 0.6$ with uniform and non-uniform optimized PTO damping

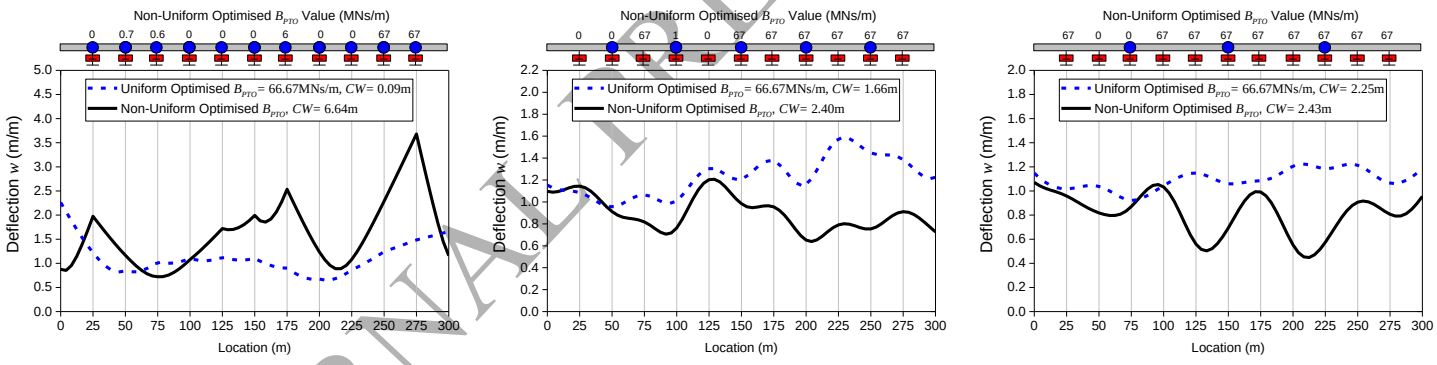

(a) Type-A: $N = 12$ Modules (b) Type-B: $N = 6$ Modules (c) Type-C: $N = 4$ Modules

Figure 19 – Hydroelastic response for Group III pontoon-type WEC under $\lambda/L = 0.8$ with uniform and non-uniform optimized PTO damping

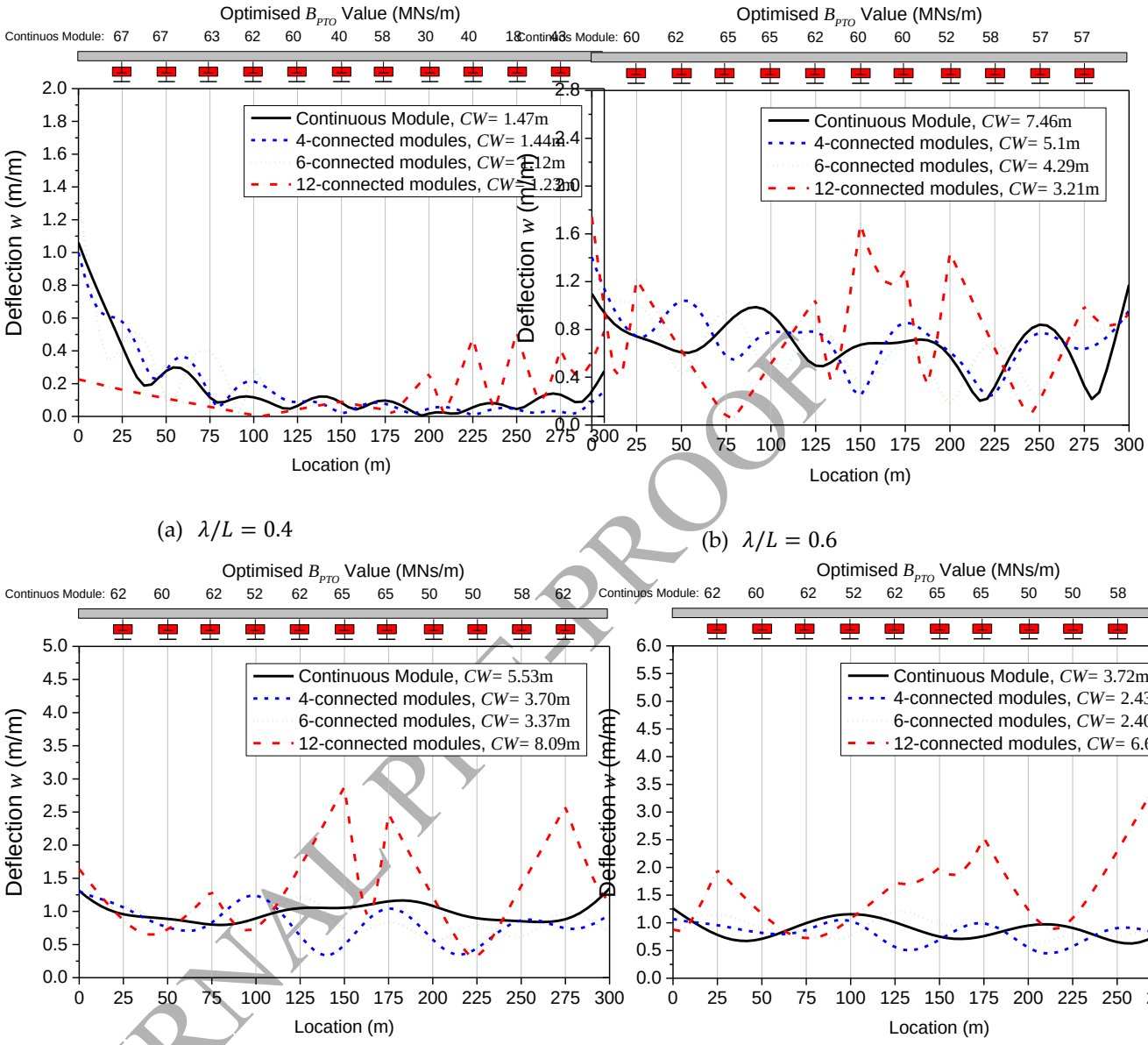

Figure 20 – Comparison of hydroelastic response for Group III continuous pontoon-type WEC with 4-, 6- and 12-connected modules under their respective optimized B_{PTO} for (a) $\lambda/L = 0.2$ and (b) $\lambda/L = 0.4$ (c) $\lambda/L = 0.6$ (d) $\lambda/L = 0.8$